JACS Au
AN OPEN ACCESS JOURNAL OF THE AMERICAN CHEMICAL SOCIETY

Open Access
This article is licensed under CC-BY-NC-ND 4.0

pubs.acs.org/jacsau
Perspective

Advancing the Understanding of Oxygen Vacancies in Ceria: Insights into Their Formation, Behavior, and Catalytic Roles

Zhong-Kang Han, Wen Liu, and Yi Gao*

Cite This: JACS Au 2025, 5, 1549−1569

Read Online
ACCESS | Metrics & More | Article Recommendations

ABSTRACT: Oxygen vacancies (O_V's) in ceria (CeO_2) are critical structural and electronic features that underpin ceria's remarkable oxygen storage capacity, redox catalytic performance, and wide-ranging applications in catalysis, solid oxide fuel cells, and gas sensors. These vacancies, which result from the removal of oxygen atoms, enable dynamic oxygen exchange between the solid and its environment, profoundly influencing ceria's catalytic properties. The intricate surface structures of ceria play a key role in determining its properties and its interactions with supported metal catalysts. Over the past decade, advancements in state-of-the-art in situ characterizations, first-principles calculations, and emerging machine learning frameworks have significantly enhanced our understanding of the formation mechanisms, behaviors, and catalytic roles of O_V's. This perspective highlights recent experimental and theoretical progress in ceria surface research, emphasizing the dynamic interplay between surface structures and reactive environments. Additionally, the perspective addresses key challenges in elucidating ceria's defect chemistry and explores opportunities to tailor its properties using multiscale modeling and AI-driven methodologies.

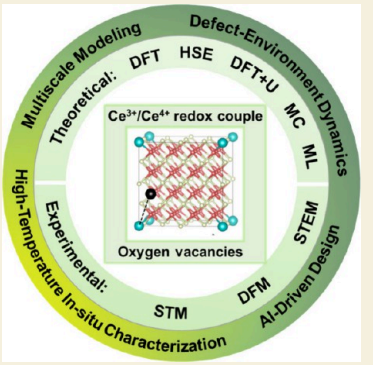

KEYWORDS: *Oxygen vacancies, polarons, surface reconstructions, dynamics, multiscale modeling*

1. INTRODUCTION

Oxygen vacancies (O_V's) in ceria (CeO_2) are central to its redox functionality and are tightly coupled to polaron formation, where electrons localize on cerium ions to form Ce^{3+} sites.[1−10] This coupling allows ceria to store and release oxygen effectively, enabling catalytic processes such as CO oxidation,[11−17] water−gas shift,[18−25] and hydrogenation reactions.[26−32] The formation of polarons in the vicinity of O_V's enhances electron transport, modulates reaction barriers, and creates unique binding sites for reactants.[33−36] Consequently, controlling the concentration and distribution of O_V's—and, by extension, the polarons associated with them—is critical for optimizing ceria's catalytic activity and stability.[37−41] Furthermore, the dynamic interplay between O_V's and polarons influences ceria's interaction with supported metals and single atoms, often resulting in synergistic effects that improve catalytic performance.[18,42−45] By dictating where and how electrons localize, O_V's regulate both the electronic structure, and the charge exchange processes at the ceria surface.[2,46,47] Recent advances in both experimental and computational techniques, ranging from in situ microscopy to advanced first-principles calculations, underscore the potential of engineering O_V's and polarons to fine-tune ceria's redox and catalytic properties.[48−51] This growing understanding paves the way for designing highly efficient CeO_2-based materials for energy and environmental applications.

Oxygen vacancies in CeO_2 exhibit remarkable complexity, driven by a combination of lattice distortions, polaron formation, and the heterogeneous coordination environments found on different crystallographic facets.[2,3,6,52−55] When an oxygen atom is removed from the CeO_2 lattice, two Ce^{4+} ions will be reduced to Ce^{3+}, creating localized charge states and lattice distortions known as polarons.[4,9,56,57] This interplay of structural and electronic effects significantly amplifies the complexity of ceria's defect chemistry. For instance, on the (111) facet, oxygen vacancies can appear as isolated vacancies, aggregated vacancy clusters, or even extended surface reconstructions.[56,58,59] Each configuration presents unique binding energies, redox potentials, and local electronic structures, influencing where and how reactants bind during catalytic processes. Such configurations can also shift dynamically in response to temperature changes or altering oxygen partial pressures, leading to a wide range of catalytic outcomes.[5,60,61] Moreover, doping ceria with transition metals or rare-earth elements can further diversify the types of vacancy structures that emerge, affecting the charge distribution and the interplay between vacancies and polarons.[62−66] This complex landscape underscores the importance of advanced computa-

Received: January 27, 2025
Revised: March 18, 2025
Accepted: March 19, 2025
Published: March 28, 2025

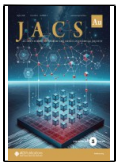

ACS Publications
© 2025 The Authors. Published by American Chemical Society

https://doi.org/10.1021/jacsau.5c00095
JACS Au 2025, 5, 1549−1569

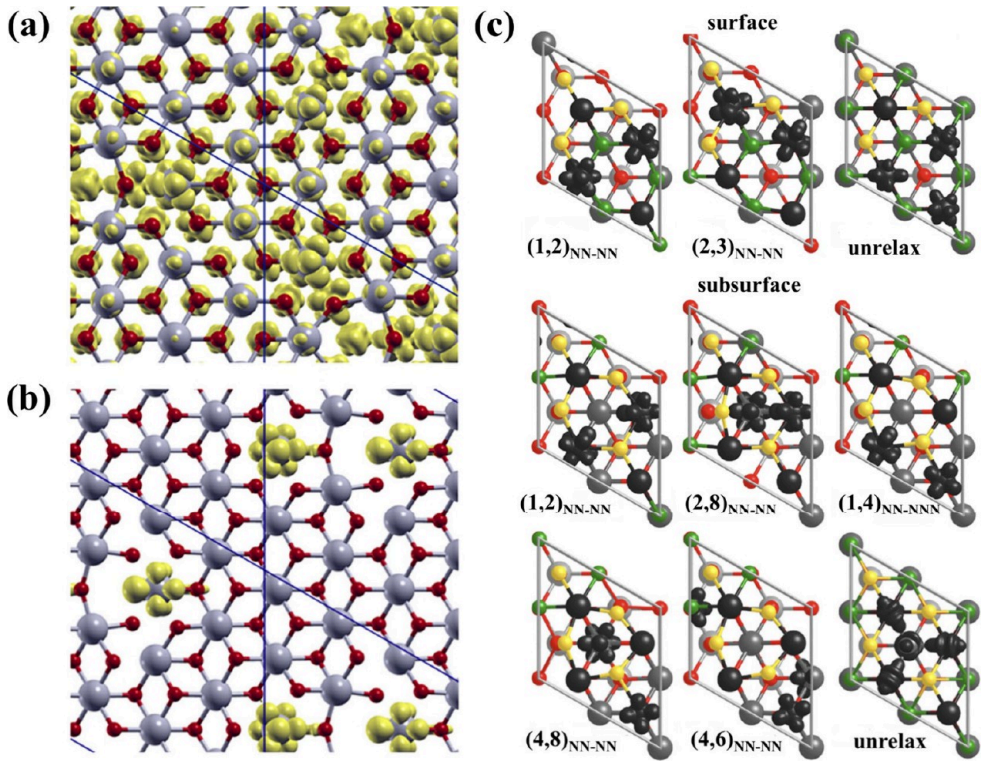

Figure 1. (a) Spin density (yellow) for a surface oxygen vacancy in CeO_2(111) obtained using PBE. (b) Spin density (yellow) for a surface oxygen vacancy in CeO_2(111) obtained using the hybrid functional HSE. Reprinted with permission from ref 7. Copyright 2013 American Chemical Society. (c) Spin density (black) for oxygen vacancies in CeO_2(111) obtained using DFT+U. Reprinted with permission from ref 79. Copyright 2009 American Physical Society.

tional and experimental approaches to accurately capture the formation energies, diffusion barriers, and local electronic states associated with oxygen vacancies. Ultimately, gaining a deep understanding of these vacancy structures is key to unlocking ceria's potential across a variety of industrially relevant applications.

Recent advances in high-resolution imaging, such as aberration-corrected scanning transmission electron microscopy (STEM), scanning tunnelling microscopy (STM), and dynamic force microscopy (DFM), have revealed that oxygen vacancies in ceria can distribute themselves in surface and subsurface layers, coalesce into linear or triangular clusters,[56] or form periodic superstructures.[67] These vacancies can even create extended one- or two-dimensional reconstructions, exemplifying how readily ceria adapts its surface stoichiometry to different environments.[68] Temperature and reactive conditions—such as hydrogen or carbon monoxide atmospheres—can further drive the dynamic rearrangement of vacancies and polarons, leading to new defect configurations with distinct catalytic properties. From a computational perspective, density functional theory (DFT) and more recent machine learning-assisted methods have begun to map out these diverse vacancy landscapes, quantifying how varying degrees of surface reduction or doping levels can stabilize specific vacancy clusters.[62,69,70] For instance, vacancy formation energies and Ce^{3+} localization patterns often shift with changing local geometry and charge distributions, resulting in pronounced site-specific behavior. This intricate variance of possible structural configurations illustrates why the complexity of oxygen vacancy configurations is so integral to ceria's multifunctional capabilities. Harnessing and tailoring this complexity—through controlled doping, precise temperature management, and reactive atmosphere design—offers an avenue to finely tune ceria for optimized performance in catalysis, solid oxide fuel cells, and other energy-related technologies. In this Perspective, we offer a comprehensive outline of recent trends and future directions in multiscale modeling, AI-driven methodologies, and combined experimental and theoretical approaches for advancing the understanding of oxygen vacancies in CeO_2.

2. ADVANCEMENTS IN COMPUTATIONAL INVESTIGATIONS OF OXYGEN VACANCIES IN CeO_2

2.1. Density Functional Theory (DFT) and Hybrid Functional Approaches

Standard DFT functionals, such as the generalized gradient approximation (GGA), often encounter notable difficulties when describing the O_V's in CeO_2. One critical challenge arises from the partially localized 4f electrons associated with reduced cerium ions (Ce^{3+}), which can be misrepresented by these functionals (Figure 1a). As a result, calculations may underestimate the energy of polaron formation or incorrectly delocalize electrons. This mismatch can, in turn, misrepresent the structural relaxations around O_V's and hinder accurate comparisons with experimental data. Additionally, the subtle interplay between lattice distortions, polaron localization, and defect energetics demands more refined methods than what standard GGA often provides. Consequently, while GGA-based DFT can offer useful preliminary insights, researchers frequently find it insufficient for achieving a comprehensive understanding of O_V formation, dynamics, and associated electronic states in CeO_2.[71,72]

Hybrid functionals, such as HSE06, offer a promising alternative by incorporating a fraction of exact Hartree−Fock

https://doi.org/10.1021/jacsau.5c00095
JACS Au 2025, 5, 1549−1569

Table 1. Formation Energy of Oxygen Vacancies (with Respect to 1/2 O_2, in eV) on the CeO_2(111) Surface in the Ferromagnetically State and Madelung Potential (in V) at the Vacant Site for Both Relaxed and Unrelaxed (HSE06) Geometries[a]

Ce^{III}	PBE + U[b]	LDA + U	HSE06	V_{Mad}^{unrel}	V_{Mad}^{rel} [c]	Ce—O
			Surface			
Unrelax	3.75	4.46				
$(1, 2)_{NN\text{-}NN}$	2.50 (2.50)	3.31	3.30	−8.60	−4.71 (−3.74)	2.36, 2.34
$(2, 3)_{NN\text{-}NNN}$	2.34 (2.30)	3.21	3.10	−10.29	−4.51 (−1.71)	2.35, 2.49
			Subsurface			
Unrelax	3.93	4.73				
$(1, 2)_{NN\text{-}NN}$	2.38 (2.40)	3.39	3.21	−10.47	−3.91 (−2.59)	2.39, 2.39
$(2, 8)_{NN\text{-}NN}$	2.40 (2.48)	3.44				
$(1, 4)_{NN\text{-}NNN}$	2.00 (2.02)	3.08	2.79	−12.12	−3.15 (−1.78)	2.38, 2.46
$(4, 8)_{NNN\text{-}NN}$	2.08 (2.11)	3.17				
$(4, 6)_{NNN\text{-}NNN}$	1.87 (1.89)	2.99	2.65	−14.61	−3.01 (−1.21)	2.47, 2.44

[a]Ce—O corresponds to the average Ce^{III}—O bond length (in Å) in the relaxed (HSE06) structures. Table reprinted with permission from ref 79. Copyright 2009 American Physical Society. [b]In parentheses, single-point calculation with a (2 × 2 × 1) k mesh and the geometry of the point optimization. [c]In parentheses, Madelung potential with Bader charges.

exchange, thereby improving the treatment of localized electronic states. This partial inclusion of exact exchange counteracts the self-interaction errors commonly encountered in standard DFT, yielding more accurate descriptions of polaronic defects and localized electrons in CeO_2 (Figure 1b). Through better alignment of the Ce 4f states, hybrid functionals produce more realistic vacancy formation energies, charge localization patterns, and structural relaxations surrounding O_V's. Consequently, these calculations often align more closely with experimental observations and allow for a refined understanding of the interplay between O_V's, polarons, and catalytic behavior.[73−78] By bridging theoretical predictions and experimental data, hybrid functionals significantly elevate the quality and credibility of insights gained in defect and catalysis research on CeO_2.

Despite their enhanced accuracy, hybrid functionals come with substantial trade-offs that can limit their practical application in large-scale or high-throughput investigations of CeO_2. First, the computational cost is notably higher than that of conventional DFT functionals, often rendering hybrid methods impractical for systems with large supercells. Second, the fraction of exact exchange included in hybrid functionals is typically treated as a tunable parameter, introducing a degree of arbitrariness. Collectively, these drawbacks mean that hybrid functionals, while more reliable for describing O_V's and polaronic states, require balancing of accuracy and efficiency. When pushed beyond their practical computational limits, researchers might need alternative or complementary methods to maintain feasibility.

2.2. Density Functional theory with Hubbard-like Correction (DFT+U)

Density functional theory plus U (DFT+U) is a refined extension of standard density functional theory, specifically designed to tackle systems featuring partially localized electronic states, such as d or f orbitals. By adding a Hubbard-like correction term denoted by the U parameter, DFT+U penalizes the occupancy of orbitals and thus better captures the localized nature of certain electrons (Figure 1c).[2,4,35,80−82] This modification significantly improves the computation of energies (Table 1), electron distributions, and local structural relaxations, often bringing theoretical results into closer agreement with experimental data. As a result, DFT+U has become a go-to method for investigating wide classes of materials, particularly those rich in strongly correlated or localized electronic states, such as transition-metal and rare-earth oxides.

In the CeO_2 O_V research, DFT+U is instrumental for several reasons. During the formation of an O_V, some Ce^{4+} ions in CeO_2 are reduced to Ce^{3+}, creating localized 4f electrons whose correct depiction is crucial for predicting defect energetics, migration barriers, and catalytic mechanisms. Standard DFT often struggles to capture these localized states and their associated polaronic effects, resulting in errors in vacancy formation energies or misplacement of the localized charges. In contrast, DFT+U provides a more accurate treatment of these effects by tuning the U parameter, refining the representation of the defect-induced electronic structure and enabling more dependable calculations of lattice relaxation. This enhanced reliability in describing O_V's and polaronic states underpins deeper insights into how these defects govern catalytic and electronic behaviors of CeO_2, thereby guiding researchers in designing advanced CeO_2-based materials for applications ranging from catalysis to energy storage.

In computational studies of O_V's in CeO_2 using DFT+U, carefully choosing an optimal U value is essential for accurately modeling the partially localized 4f electrons and the polaronic effects they introduce. Researchers typically select U values in the range of 4.0 to 5.5 eV, with 5.0 eV commonly recommended for correcting self-interaction errors that conventional DFT often overlooks.[4,9,82] This approximate range is generally validated by comparing calculated properties—such as lattice parameters and band gaps—to experimental benchmarks. Consequently, a U value of around 5.0 eV is broadly accepted as a balanced choice, maintaining computational efficiency while delivering faithful representations of Ce^{3+} states and the energetics associated with oxygen defects in CeO_2.

The complexity of CeO_2's defect chemistry—spanning multiconfigurational O_V states, polaron localization, and dopant-vacancy interactions necessitates methods beyond static DFT calculations. Monte Carlo (MC) simulations and machine learning (ML) approaches have emerged as powerful tools for modeling thermally activated processes and configurational entropy effects.[52,83−88] MC methods utilize stochastic sampling and statistical averaging to resolve high-dimensional or probabilistic problems, offering robust capabilities for uncertainty quantification. In CeO_2 research, this approach is pivotal for probing the thermodynamic stability and statistical distribution of O_V configurations under varying conditions (e.g.,

https://doi.org/10.1021/jacsau.5c00095
JACS Au 2025, 5, 1549−1569

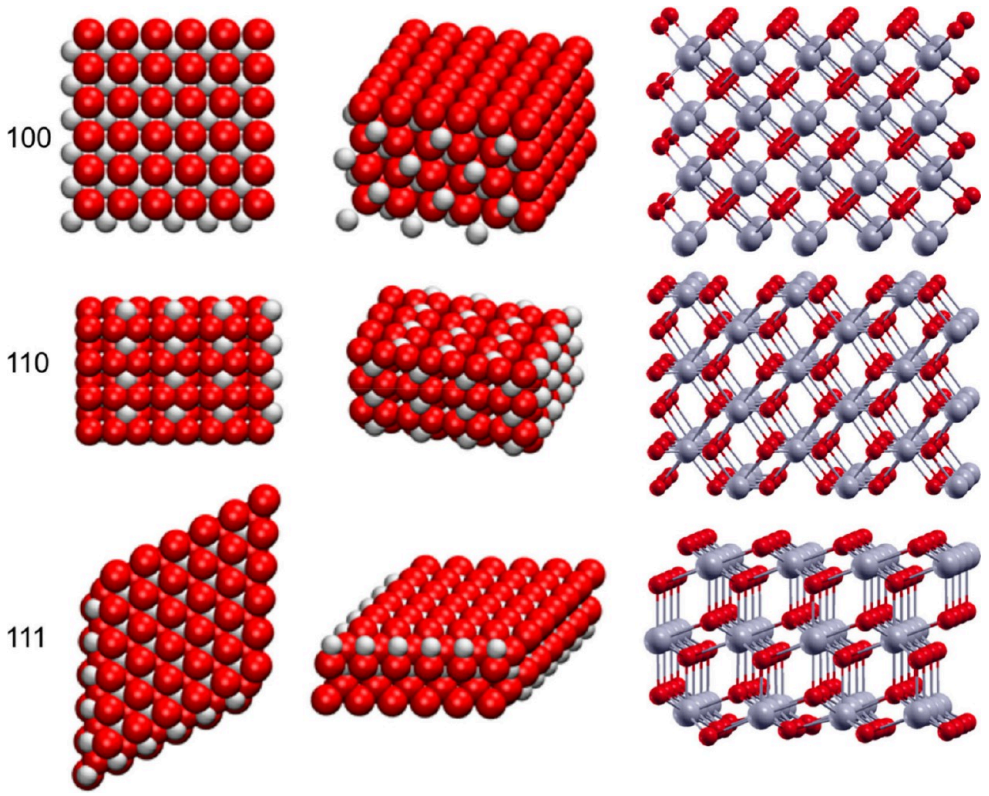

Figure 2. Top, side, and perspective view of CeO_2 facets (100), (110), and (111). Cerium and oxygen ions are represented by gray and red spheres, respectively. Reprinted with permission from ref 92. Copyright 2017 American Chemical Society.

temperature, oxygen partial pressure).[52] ML approaches, particularly machine learning potentials, effectively bridge the gap between quantum-mechanical accuracy and large-scale atomistic simulations.[87−89] Together, these methods offer efficient solutions for understanding oxygen defect chemistry, which is crucial for catalyst design.

3. FORMATION, DISTRIBUTION, AND DYNAMICS OF OXYGEN VACANCY

3.1. Oxygen Vacancy Formation Energies on Different Surface Facets and in the Bulk

O_V formation demands relatively high energy in the bulk region of CeO_2, often reported between 2.5 eV and 3.5 eV in DFT+U calculations.[9] This high formation energy primarily arises from the strong lattice stability of the fluorite structure, where each oxygen atom is tightly coordinated to surrounding cerium cations. Because of these robust local bonds, creating a vacancy in the bulk requires breaking multiple Ce−O bonds, making the process energetically more expensive compared to surface vacancy formation. However, at elevated temperatures or under highly reducing environments, bulk vacancies can still form and disappear in a dynamic process that underpins ceria's ability to store and release oxygen. This oxygen buffering capacity is crucial in applications such as solid oxide fuel cells, where efficient ionic conduction is needed. Moreover, the high vacancy formation energy in the bulk contributes to ceria's excellent structural integrity under aggressive conditions involving high temperatures, redox cycling, or oxidative atmospheres. Even if some vacancies form, the overall lattice remains stable due to the robust fluorite framework. In doped ceria, aliovalent cations may alter the vacancy formation energy by inducing local lattice distortions, yet the intrinsic energy cost for generating bulk vacancies typically remains higher than on ceria surfaces. Consequently, many catalytic and electrochemical reactions predominantly take advantage of surface or near-surface O_V's, as these are more easily formed and annihilated.

The (111) surface of ceria (Figure 2) is widely recognized as its most thermodynamically stable facet, characterized by a densely packed arrangement and relatively low surface energy. According to DFT+U calculations, O_V formation energies for this facet (Table 2) generally lie between 1.8 eV and 2.8 eV,[90,91] a notable reduction compared to the bulk. This lower energy stems from the diminished coordination of surface oxygen atoms, which are less tightly bound and therefore easier to remove or exchange. As a result, the (111) surface can readily form and annihilate O_V's, facilitating redox reactions such as CO oxidation, water−gas shift, and even partial oxidation of hydrocarbons. While the (111) surface is often deemed less reactive than the more open (110) and (100) facets, its strong thermodynamic stability ensures it predominates under equilibrium conditions and during prolonged operation at high temperatures. This stability is a key factor in many catalytic processes that require robust, long-lasting performance. Furthermore, slight surface modifications—such as introducing noble metal particles or doping with aliovalent cations—can enhance its vacancy formation and improve catalytic activity without significantly compromising its structural integrity.

In contrast to the stable (111) surface, the (110) facet of ceria features a higher density of undercoordinated cerium and oxygen atoms, which translates to lower O_V formation energies (Table 2), typically ranging from 1.0 eV to 2.5 eV.[91,93,94] This reduced vacancy formation energy arises from weaker bonding environments that make it easier to create and annihilate oxygen vacancies. As a direct consequence, the (110) surface often

https://doi.org/10.1021/jacsau.5c00095
JACS Au 2025, 5, 1549−1569

Table 2. Formation Energy of Surface (V^A) and Subsurface (V^B) Oxygen Vacancies (with Respect to 1/2 O_2, in eV) at Ceria Surfaces[a]

	111 facet		110 facet		100 facet	
	2 × 2 unit cells	3 × 3 unit cells	2 × 2 unit cells	4 × 2 unit cells	p(2 × 2) unit cells	c(2 × 2) unit cells
			Vacancy type V^A			
E_f^{unrel}	3.79		3.41		2.61	
E_f	2.22	1.96	1.29	1.06	1.78	1.35
ΔE_f^{relax}	1.57		2.12		0.83	
Ce^{3+} (n, m)	$(2, \bar{2})$	(2, 2)	(1, 2)	(1, 2)	$(1, \bar{2})$	(1, 1)
			Vacancy type V^B			
E_f^{unrel}	4.01		4.47		3.86	
E_f	1.81	1.76	2.17	2.29	1.75	1.82
ΔE_f^{relax}	2.20		2.30		2.11	
Ce^{3+} (n, m)	$(2, \bar{2})$	(2, 2)	(2, 2)	(1, 2)	$(2, \bar{2})$	(1, 2)

[a] E_f^{unrel} and E_f correspond to the values for the unrelaxed and relaxed structures, respectively. ΔE_f^{relax} corresponds to the energy gained from lattice relaxations upon vacancy formation. Ce^{3+} (n, m) indicates the positions of the Ce^{3+} ions in the relaxed structures. Table reprinted with permission from ref 91. Copyright 2021 IOP Publishing Ltd.

exhibits enhanced catalytic reactivity, particularly for reactions requiring swift oxygen exchange, such as CO oxidation and hydrogenation.[95,96] The abundance of low-coordination sites can also lead to stronger adsorption of reaction intermediates, providing additional catalytic benefits and increasing turnover frequencies. However, it is thermodynamically less stable than (111). Under near-equilibrium conditions, the ceria crystal structure tends to minimize its surface energy, leading to a smaller population of (110) facets. Nonetheless, nonequilibrium environments—such as rapid redox cycling, elevated temperatures, or the presence of strong adsorbates—can promote the formation or exposure of (110) surfaces. Even transient emergence of this facet can greatly impact overall catalytic performance, as the (110) surface may provide a dominant pathway for oxygen exchange and the activation of small molecules. Thus, while it may not always be the most visible facet under routine conditions, the (110) surface is recognized as a key driver in enhancing ceria's redox behavior, underlining its pivotal role in catalytic applications where oxygen mobility is critical.

The (100) surface of ceria occupies an intermediate position between the highly reactive (110) facet and the more stable (111) facet, with reported O_V formation energies (Table 2) generally lying in the 1.3 eV to 2.4 eV range.[91,92,97,98] Although its surface energy is higher, causing it to be less abundant under equilibrium conditions, the (100) facet's cubic atomic arrangement offers substantial flexibility in accommodating vacancies. This structural adaptability enables notable local relaxations around missing oxygen atoms, reducing the energy cost associated with vacancy formation. Consequently, the (100) surface can exhibit appreciable activity in catalytic transformations such as hydrocarbon reforming, selective oxidation, and partial hydrogenation. Despite its relatively high surface energy, the (100) facet may become significant under certain reaction conditions, where surface reconstructions or energetic interactions with adsorbates tilt the balance in favor of less stable but more reactive facets.[68,99,100] Furthermore, doping or depositing secondary metals can modulate vacancy formation energies on the (100) surface, refining its catalytic properties for specialized applications.[101,102]

3.2. Interactions and Distributions of Oxygen Vacancies

Among the various crystal facets of CeO_2, the (111) surface is most investigated because it is the thermodynamically most stable and thus predominates under typical growth and operating conditions. This stability, combined with a well-defined atomic arrangement, enables easier experimental characterization and more straightforward theoretical modeling. Therefore, in our discussion, we also focus primarily on the (111) facet, while acknowledging that other surfaces of ceria can exhibit distinct structural and catalytic properties. The work by

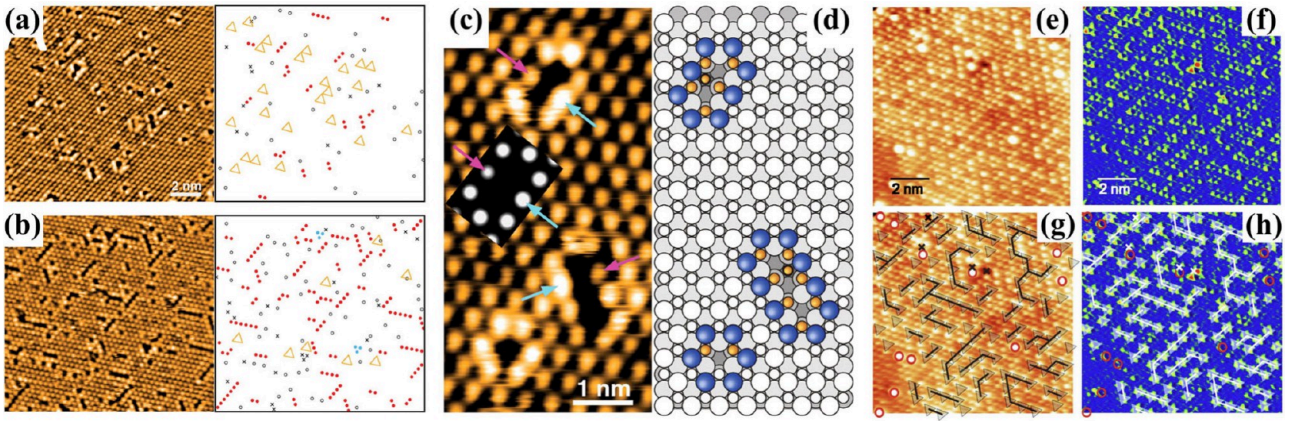

Figure 3. (a, b) STM images of the CeO_2(111) surface obtained after 1 min (a) and 5 min (b) of annealing at 900 °C, with corresponding representations of the observed defects. (c) STM image of a double and a triple linear surface oxygen vacancy cluster as well as a simulated STM image of a double linear surface oxygen vacancy cluster (inset). The characteristic unit (magenta and cyan arrows) is an indication of the presence of a subsurface vacancy in every linear surface oxygen vacancy clusters. STM imaging conditions: −3.0 V, 0.1 nA. (d) Corresponding structural model. (a–d) Reprinted with permission from ref 56. Copyright 2005 American Association for the Advancement of Science. Topographic (e) and dissipation (f) images of a slightly reduced CeO_2(111) surface area. (g, h) Images shown in (e) and (f) where the association between the observed surface structure and the type of defect has been depicted. Triangles, crosses, and circles correspond to subsurface oxygen vacancies, surface oxygen vacancies, and hydroxide defects, respectively. The lines over both images highlight the arrangement observed for the subsurface oxygen vacancy structures. (e–h) Reprinted with permission from ref 67. Copyright 2007 American Physical Society.

https://doi.org/10.1021/jacsau.5c00095
JACS Au 2025, 5, 1549−1569

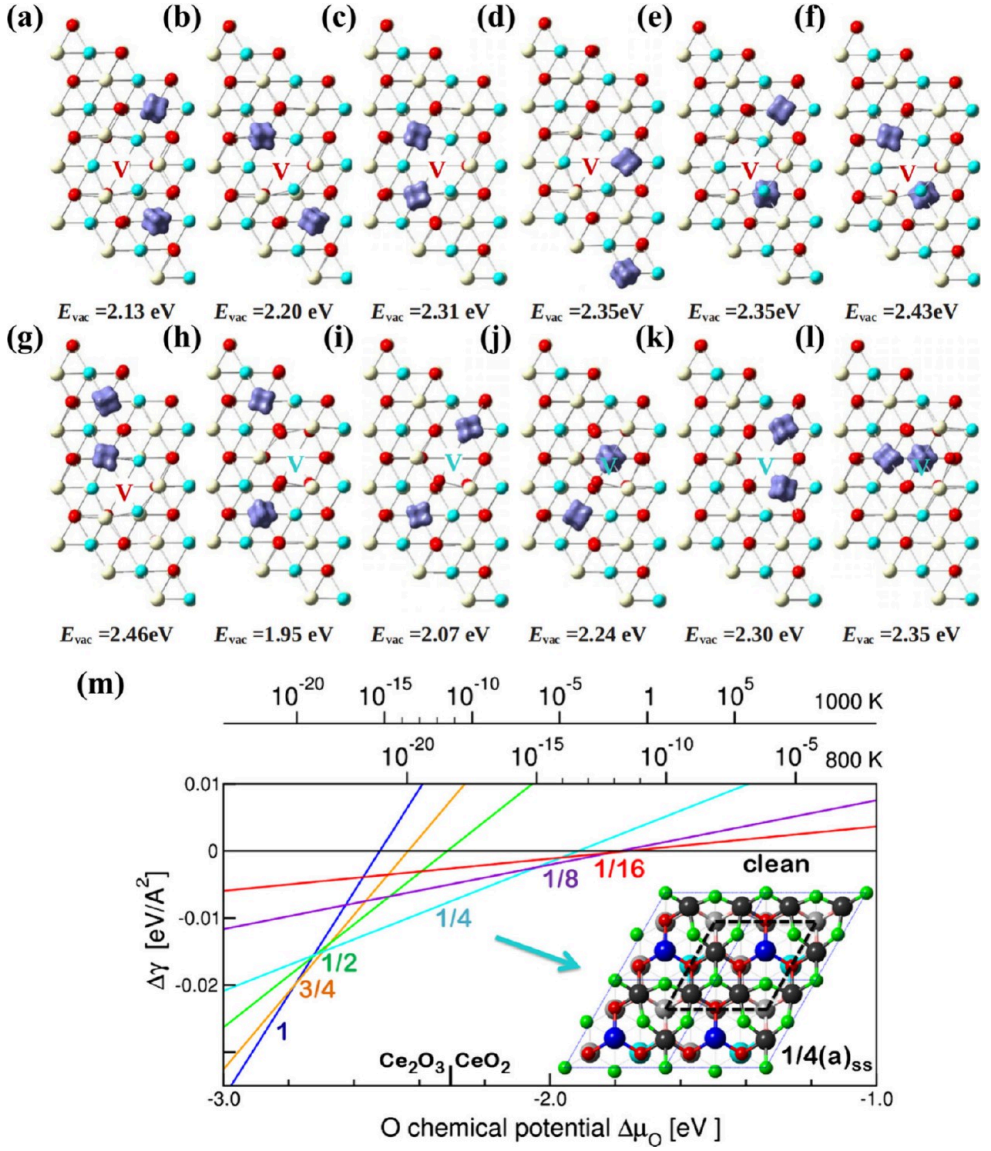

Figure 4. Top view of the $CeO_2(111)$ surface with a single O vacancy on the top-surface (a–g) and subsurface (h–l) and the corresponding calculated vacancy formation energies (E_{vac}). They are at two second-neighbor (a) Ce^{3+}, (b) first- and second-neighbor Ce^{3+}, (c) two first-neighbor Ce^{3+}, (d) first- and forth-neighbor Ce^{3+}, (e) first-neighbor Ce^{3+} in the second Ce layer and second-neighbor Ce^{3+}, (f) first-neighbor Ce^{3+} in the second Ce layer and first-neighbor Ce^{3+}, (g) first- and third-neighbor Ce^{3+}, with respect to the top-surface O vacancy; and (h) two second-neighbor Ce^{3+}, (i) separated first- and second-neighbor Ce^{3+}, first-neighbor Ce^{3+} in the second Ce layer and (j) second-neighbor Ce^{3+}, (k) two first-neighbor Ce^{3+}, (l) first-neighbor Ce^{3+} in the second Ce layer and first-neighbor Ce^{3+}, with respect to the subsurface O vacancy. Cerium, O on top-surface, and O on subsurface are represented by white, red, and blue spheres, respectively. Red V represents top-surface O vacancy, and light-blue V represents subsurface O vacancy. The isosurface (0.05 e/Å^3) of calculated spin charge densities are in dark blue. (a–i) Reproduced with permission from ref 103. Copyright 2009 American Physical Society. (m) Free energy change of surface $\Delta\gamma$ as a function of the oxygen chemical potential $\Delta\mu$O for different vacancy concentrations. Top x axis is the pressure scale (in atmospheres) assuming ideal gas behavior. The enthalpy and entropy at T = 800 and 1000 K were calculated using tabulated values. The dashed lines in the $1/4(a)_{ss}$ structure show the (2×2) local arrangement of subsurface vacancies. The surface (subsurface) oxygen atoms are represented by green (red). Ce^{4+} ions at the second (fifth) atomic layer are represented by dark gray (light gray). Ce^{3+} ions at the second (fifth) atomic layer are represented by blue (light blue). Reproduced with permission from ref 90. Copyright 2013 American Physical Society.

Esch and co-workers investigates the atomic-scale mechanisms of O_V formation on CeO_2, a critical aspect of its performance in catalytic applications.[56] Using high-resolution scanning tunneling microscopy (STM) at ~600 K and density functional theory (DFT), the authors found surface O_V's on the $CeO_2(111)$ surface are slightly more stable than subsurface O_V's under certain conditions (Figure 3a). This relative stability is evidenced by the higher occurrence of surface vacancies compared to subsurface vacancies on slightly reduced surfaces, as observed in high-resolution STM. As shown in Figure 3b, at higher vacancy concentrations, vacancy clusters formed and the experimental results reveal that the localization of electrons left by removed oxygen atoms plays a pivotal role in the formation and stabilization of vacancy clusters. These clusters predominantly expose reduced Ce^{3+}. Notably, subsurface vacancies are essential for the formation of linear surface vacancy clusters (LSVCs). LSVCs on the $CeO_2(111)$ surface exhibit distinctive structural features that are critical to their formation. These

https://doi.org/10.1021/jacsau.5c00095
JACS Au 2025, 5, 1549–1569

clusters are composed of linear arrangements of oxygen vacancies, involving both surface and subsurface vacancies, and are exclusively coordinated by reduced cerium ions Ce^{3+}, with no neighboring Ce^{4+} ions. A unique characteristic of LSVCs is the presence of a pair of rim oxygen atoms that diffuse in opposite directions: one atom relaxes outward while the other relaxes inward toward the surface (Figure 3c and 3d). This asymmetric relaxation creates a structural unit that is consistently observed within LSVCs.

Torbrügge et al. investigated the structural and electronic properties of surface and subsurface O_V's on the slightly reduced $CeO_2(111)$ surface using dynamic force microscopy (DFM) at low temperatures (80 K).[67] Surface O_V's are identified as missing oxygen atoms surrounded by six protruding neighbors, exhibiting relaxation patterns predicted by first-principles calculations. Subsurface O_V's, located in the third atomic layer, are observed as three oxygen atoms protruding from the surface, with localized electrons reducing nearby Ce^{4+} ions to Ce^{3+}. The main finding is the ordering of subsurface O_V's into linear arrays, driven by a balance of short-range attractive and repulsive interactions (Figure 3e–h). These vacancies do not cluster densely, but form ordered patterns, leaving defect-free areas in between. The two experimental studies on O_V's in $CeO_2(111)$ surfaces present conflicting observations regarding the stability and distribution of surface and subsurface vacancies. In the work by Esch et al., it is suggested that surface and subsurface O_V's are nearly equally stable, with similar formation energies.[56] However, the study by Torbrügge et al. challenges this, providing evidence of distinct differences in stability and behavior between surface and subsurface vacancies. Using atomic resolution DFM at low temperatures, the authors identify unique ordering patterns of subsurface vacancies.[67] This discrepancy highlights the complexities in understanding O_V formation and behavior, which may arise from variations in experimental conditions, such as temperature and reduction levels, or differences in the sensitivity of characterization techniques.

Theoretical studies, particularly those using DFT+U, have deepened our understanding of O_V structures on the $CeO_2(111)$ surface. These studies emphasize the intricate interplay between structural relaxations and electronic effects caused by the vacancies. When an oxygen atom is removed, two excess electrons are introduced into the lattice, and these electrons localize on near Ce ions, transforming them from Ce^{4+} to Ce^{3+}. As shown in Figure 4, the exact localization of these electrons is influenced by the local atomic environment and has been shown to lead to multiple energetically favorable configurations.[79,103] The inclusion of the Hubbard U term enhances the accuracy of these models by correcting for the electron correlation effects inherent to the Ce 4f orbitals, enabling a more realistic representation of the electronic structure of reduced CeO_2. This detailed understanding not only helps identify stable vacancy configurations but also sheds light on how these defects influence the overall properties of CeO_2. With DFT+U calculations, these theoretical models have reproduced several critical experimental findings, including the visibility of O_V's in STM images and their influences on the surrounding lattice structure. A notable result from both theory and experiment is the preferential stability of subsurface O_V's over surface O_V's under reducing conditions.[90] This theoretical prediction aligns well with advanced DFM experiments that reveal a predominance of subsurface defects in reduced CeO_2 samples. Additionally, calculations have predicted vacancy-induced lattice relaxations and ordered vacancy arrangements, such as the (2×2) periodic pattern observed in DFM studies (Figure 4m).[90] This work also shows spatial and electronic correlations between oxygen vacancies and associated Ce^{3+} ion pairs aligning with STM research conducted by Jerratsch et al.[104] They demonstrated that Ce^{3+} ions do not preferentially occupy nearest-neighbor positions relative to oxygen vacancies, favoring instead second- or third-neighbor configurations. This behavior arises from the interplay between electrostatic repulsion and lattice relaxation effects, which stabilize nonadjacent Ce^{3+}-O_V arrangements. These results not only validate the predictive power of DFT+U but also demonstrate its utility in uncovering atomic-scale mechanisms that are challenging to resolve experimentally. Despite the overall agreement between theoretical and experimental findings, certain discrepancies persist, highlighting the complexities of accurately modeling oxygen vacancies. For instance, STM studies by Esch et al. have reported an almost equal distribution of surface and subsurface O_V's under specific experimental conditions.[56] However, DFT+U calculations consistently indicate that subsurface O_V's are energetically more favorable, suggesting that these should dominate under reducing conditions. This divergence could arise from the inherent limitations of computational models, such as the neglect of finite-temperature effects, entropic contributions, or the influence of surface adsorbates, which can significantly alter the vacancy distribution. And the incorrect structural models may be used to interpret experimental observations. To address these issues, more effort may need to integrate statistical thermodynamic approaches to capture the temperature-dependent behavior of vacancies and resolve these discrepancies between theoretical predictions and experimental observations.

A novel structural model has been proposed to resolve the discrepancies observed in STM and DFM experiments on $CeO_2(111)$ surfaces. The study by Kullgren et al. introduced the idea that other species, such as fluorine impurities, could mimic the appearance of oxygen vacancies in STM experiments (Figure 5a).[105] Fluorine, for instance, shows similar electronic and topographic features in simulated STM images due to its electronic structure and interaction with the CeO_2 lattice. This model better aligns with experimental findings, such as the increased surface defect concentration upon annealing and the observed defect immobility, which are inconsistent with O_V behavior. Another alternative theoretical model is the hydroxyl-

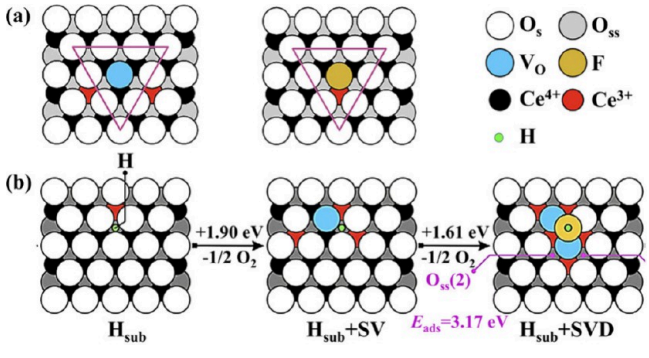

Figure 5. (a) Schematic plan views (upper row) of fluorine impurities model. Reprinted with permission from ref 105. Copyright 2014 American Physical Society. (b) Schematic plan views (bottom row) hydroxyl-vacancy model. Reprinted with permission from ref 106. Copyright 2016 American Physical Society.

https://doi.org/10.1021/jacsau.5c00095
JACS Au 2025, 5, 1549−1569

vacancy model (Figure 5b).[106] According to this model, hydroxyl groups play a critical role in stabilizing O_V's and vacancy clusters. Specifically, the coexistence of hydroxyls and O_V's significantly reduces the formation energy of vacancy clusters, making linear surface vacancy clusters (LSVCs) and triangular surface vacancy trimers (TSVTs) energetically favorable. This model aligns with STM observations, such as the prevalence of LSVCs and specific TSVT configurations. By incorporating the mutual stabilization effects between hydroxyls and O_V's, this theoretical framework effectively reproduces the STM experimental observations, providing deeper insights into the dynamic nature of $CeO_2(111)$ surface defects. However, these two new structural models fail to account for a distinctive feature of linear surface vacancy clusters (LSVCs) observed in STM experiments: the presence of a pair of rim oxygen atoms that diffuse in opposite directions, with one atom relaxing outward and the other moving inward toward the surface.

To resolve discrepancies observed in prior STM and DFM experiments, Han and co-workers systematically investigate the structural arrangements of O_V's on $CeO_2(111)$ surfaces under a wide range of temperatures and O_V concentrations (Figure 6).[52] Using a combination of DFT calculations and Monte Carlo simulations, the researchers develop a unified framework to better understand the complex vacancy behavior. They identify a new structural configuration, termed the "most stable double linear surface vacancy cluster" (ms-dLSVC), which includes two surface O_V's and one subsurface O_V (Figure 6a). This model successfully explains a key feature observed in STM experiments: the presence of rim oxygen atoms that relax in opposite directions, with one moving outward and the other inward toward the surface (Figure 6b).

Monte Carlo simulations reveal additional insights into the temperature-dependent and vacancy concentration-dependent structures of O_V distributions. At low temperatures and low O_V concentrations, the simulations show that vacancies preferentially occupy subsurface sites and form a local (2×2) ordering (Figure 7). This finding aligns with the observations from DFM experiments and suggests that the system's thermodynamic stability favors subsurface vacancies under these conditions. However, at higher temperatures and higher vacancy concentrations, surface O_V's aggregate into linear clusters, which is consistent with STM observations (Figure 7). The ms-dLSVC configuration is shown to exhibit enhanced thermodynamic stability compared to triangular trimer vacancy configurations due to its ability to release local lattice strain. These findings not only reconcile the discrepancies between experimental methods but also highlight the importance of vacancy-induced lattice relaxation in determining surface structures.

DFT+U studies reveal O_V's in $CeO_2(111)$ critically alter surface reactivity by modifying electronic structures.[107] O_V's generate Ce^{3+} ions, redistributing electron density to adjacent oxygen atoms. This weakens O−H bonds, reducing H adsorption energy and destabilizing surface-bound H. Also, the interactions between oxygen vacancies (O_V-O_V), between oxygen vacancies and Ce^{3+} ions (O_V-Ce^{3+}), and between Ce^{3+} ions themselves (Ce^{3+}-Ce^{3+}), including their many-body interactions, play a critical role in determining the structure of O_V's.[108] However, disentangling the individual contributions of these interactions remains a significant challenge. The study by Zhang et al. employed a compressed sensing-assisted cluster expansion (CE) model to address the challenges in understanding O_V structures (Figure 8).[84] Traditional methods faced difficulties in accurately sampling the electronic configurations

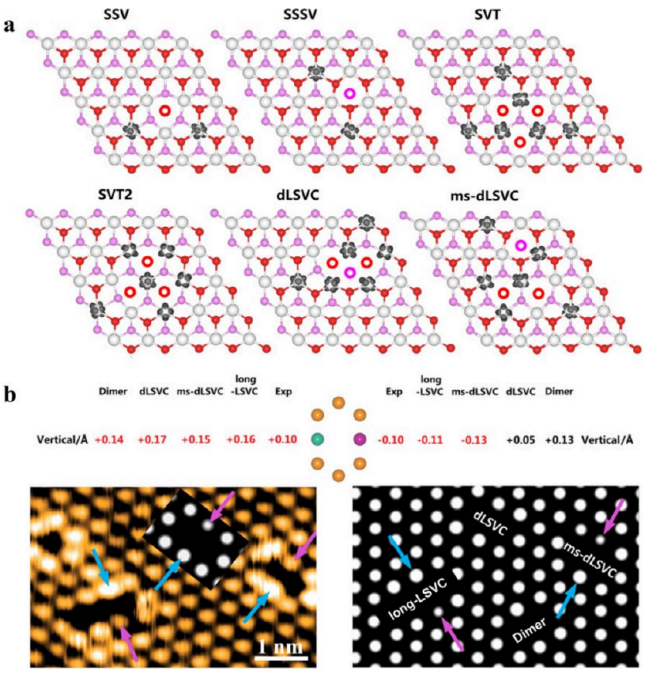

Figure 6. (a) Most stable single vacancy and trimeric vacancy structures on $CeO_2(111)$. SSV, SSSV, SVT, dLSVC, and ms-dLSVC stand for single surface vacancy, single subsurface vacancy, surface vacancy trimer, double linear surface vacancy cluster, and most stable double linear surface vacancy cluster, respectively. Cerium, surface oxygen, and subsurface oxygen atoms are depicted in white, red, and pink, respectively. Open circles represent oxygen vacancies. For clarity, only the first O−Ce−O trilayer is shown. The spin density is shown as the gray clouds localized on cerium cations. (b) Top panel: Vertical displacement of surface O atoms in SVCs. Schematic representations of the vertical movement of the oxygen atom pair formed by the cyan and magenta atoms upon formation of vacancy clusters, namely, dimer, dLSVC, ms-dLSVC, and long-LSVC. The outward and downward relaxations are denoted with + or − signs, respectively. Values consistent with experimental observation are highlighted in red. Bottom panel: Experimental image from ref 56 and simulated STM images of vacancy structures on reduced $CeO_2(111)$. The height of the tip in the constant-height mode simulated images is ∼0.6 Å. The insert displays the simulated STM image of the dLSVC structure by Esch et al. with all Ce^{3+} ions in nearest-neighbor positions to the vacancies. Experimental STM image reprinted with permission from ref 56. Copyright 2005 American Association for the Advancement of Science. Reproduced with permission from ref 52. Copyright 2018 American Physical Society.

due to the complex many-body interactions among O_V's and Ce^{3+}. By combining statistical learning and first-principles calculations, the researchers decoupled these interactions, effectively isolating the key contributions of O_V-O_V, O_V-Ce^{3+}, and Ce^{3+}-Ce^{3+} interactions. This approach identified specific configurations characterized by energetically favorable attractions and minimized repulsions, which are critical for stabilizing vacancy structures (Figure 8f and 8g).

The study revealed that O_V's tend to aggregate and favor the subsurface or third oxygen layer instead of the surface, particularly at high O_V concentrations. This finding diverges from earlier studies that primarily focused on surface and subsurface vacancy distributions. The observed preference for deeper vacancy aggregation is attributed to significant geometric relaxation effects, which had been overlooked in prior work. These insights were supported by extensive Monte Carlo simulations and validated against DFT+U calculations, demon-

https://doi.org/10.1021/jacsau.5c00095
JACS Au 2025, 5, 1549−1569

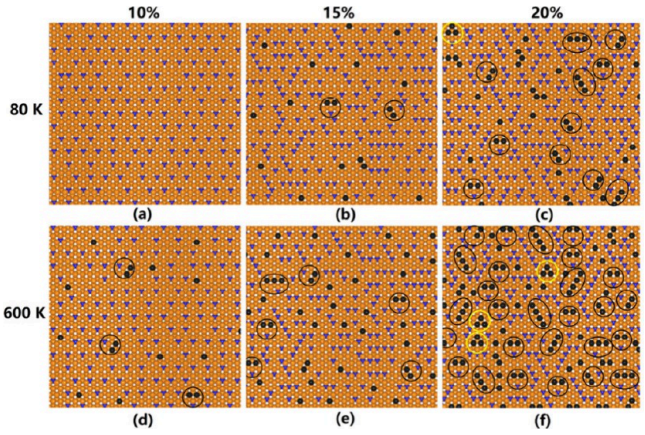

Figure 7. Monte Carlo simulated structures of a slightly (10%), moderately (15%), and highly (20%) reduced $CeO_2(111)$ surface. (a–c) 80 K and (d)-(f) 600 K. Images are to be compared with the experimental STM images in ref.[56] Oxygen atoms, surface oxygen vacancies, and subsurface oxygen vacancies are represented as orange, black, and blue balls, respectively. Cerium atoms are not shown for clarity. The ms-dLSVCs and long LSVCs are indicated with black circles. The SVTs are indicated with yellow circles. Reproduced with permission from ref 52. Copyright 2018 American Physical Society.

strating the robustness of the cluster expansion model. overall, this work provides a new theoretical framework for understanding the stability and distribution of vacancies in reducible oxides like CeO_2. The findings highlight the critical role of decoupling many-body interactions and geometric relaxation in shaping vacancy configurations, offering a refined understanding that aligns with experimental observations.

The structure of O_V's in bulk ceria is relatively less significant compared to those on the surface, and as a result, studies on bulk O_V's are comparatively scarce. However, the structure and dynamic behavior of bulk O_V's are crucial for understanding and improving the performance of solid oxide fuel cells. The study by Li et al. focuses on unraveling the structural and energetic interplay of O_V's in bulk ceria. As shown in Figure 9, using a combination of first-principles calculations and machine learning-assisted cluster expansion models, the authors systematically analyze O_V configurations and their interactions with surrounding Ce^{3+} ions.[85] The study reveals that O_V-O_V interactions play a dominant role in determining the structural stability of ceria, while O_V-Ce^{3+} interactions are secondary, and Ce^{3+}-Ce^{3+} interactions have minimal impact. By identifying key interaction types and correlating structural stability with electronic properties, the research provides a detailed understanding of how defect structures form and stabilize under varying conditions.

3.3. Dynamics of Oxygen Vacancies

O_V dynamics, specifically the mobility and transport pathways of these defects, play a critical role in determining ceria's catalytic and functional performance.[34,35,107,109−113] The diffusion rate of O_V's governs the kinetics of oxidation and reduction processes, significantly influencing reaction rates at both the surface and subsurface levels. Enhanced vacancy mobility accelerates the turnover of redox cycles, thereby improving catalytic efficiency in applications such as solid oxide fuel cells, automotive exhaust aftertreatment, and chemical synthesis. A deeper understanding of the diffusion mechanisms, facilitated by atomistic simulations and advanced experimental techniques, provides a foundation for optimizing catalytic performance. Elucidating the critical migration pathways and associated energy barriers offers opportunities to fine-tune ceria's functional properties.

O_V diffusion is a critical process influencing ceria's catalytic and functional properties, yet the precise mechanisms remained unclear. Using first-principles calculations for O_V diffusion on $CeO_2(111)$, Li et al. uncovered a novel two-step exchange mechanism for O_V diffusion.[113] As show in Figure 10, a subsurface oxygen atom fills a surface vacancy, creating a new subsurface vacancy, which is subsequently filled by a neighboring surface oxygen atom. This two-step process was found to have significantly lower energy barriers (0.44 and 0.61 eV for each step, respectively) compared to the traditional hopping mechanism, which has a barrier of 1.60 eV. The authors demonstrated that the two-step exchange mechanism is approximately 8 orders of magnitude faster than the hopping mechanism at 500 K, highlighting its practical significance in surface processes.

However, the migration mechanism of O_V's is inherently complex and is significantly influenced by the distribution of Ce^{3+} ions. Zhang et al. unravel the anomalous O_V diffusion mechanism in reduced $CeO_2(111)$ surfaces, focusing on the interplay between O_V's and polarons (Ce^{3+}).[34] The authors utilized DFT combined with ab initio molecular dynamics (AIMD) simulations to explore the dynamic interactions between O_V's and Ce^{3+} polarons across a range of temperatures. The study identifies two distinct mechanisms: a "nearest-neighbor polaron-hindered mechanism", where nearby polarons impede vacancy migration by creating energetically unfavorable pathways, and a "nearest-neighbor polaron-promoted mechanism", where polarons lower migration energy barriers and facilitate vacancy movement from subsurface to surface layers (Figure 11). These mechanisms underline the role of local polaron distribution in vacancy dynamics.

At lower temperatures, O_V migration is limited by restricted polaron motion, resulting in localized O_V's movement. As temperature increases, polarons hop more frequently, dynamically altering the energy landscape and enabling long-distance O_V's migration. However, at very high temperatures, excessive polaron hopping disrupts coordinated vacancy motion. AIMD simulations reveal that migration pathways are strongly influenced by the configuration of Ce^{3+} polarons, with vacancies preferentially migrating across Ce^{4+}-Ce^{4+} pairs due to lower energy barriers. This study provides critical insights into the entangled dynamics of O_V's and polarons, offering a microscopic framework for understanding charge and ionic transport in ceria-based materials.

3.4. Oxygen Vacancy Engineering

Engineering O_V's on ceria surfaces is a critical strategy for enhancing its catalytic and functional properties, with strain and doping emerging as two critical approaches.[54,62,114−120] Strain introduces lattice distortions that can modulate the electronic structure and alter the formation and migration energies of O_V's. Doping further complements strain engineering by introducing different cation species that alter the local electronic environment and defect chemistry. Dopants with lower oxidation states, such as trivalent lanthanides (e.g., Gd^{3+}, Sm^{3+}),[121] can induce charge compensation mechanisms that enhance vacancy concentrations. Meanwhile, aliovalent doping not only influences vacancy formation but also governs their spatial distribution and mobility, creating pathways for optimized oxygen transport.[122] Synergistically, doping can interact with strain effects, as dopants often induce localized lattice distortions

https://doi.org/10.1021/jacsau.5c00095
JACS Au 2025, 5, 1549−1569

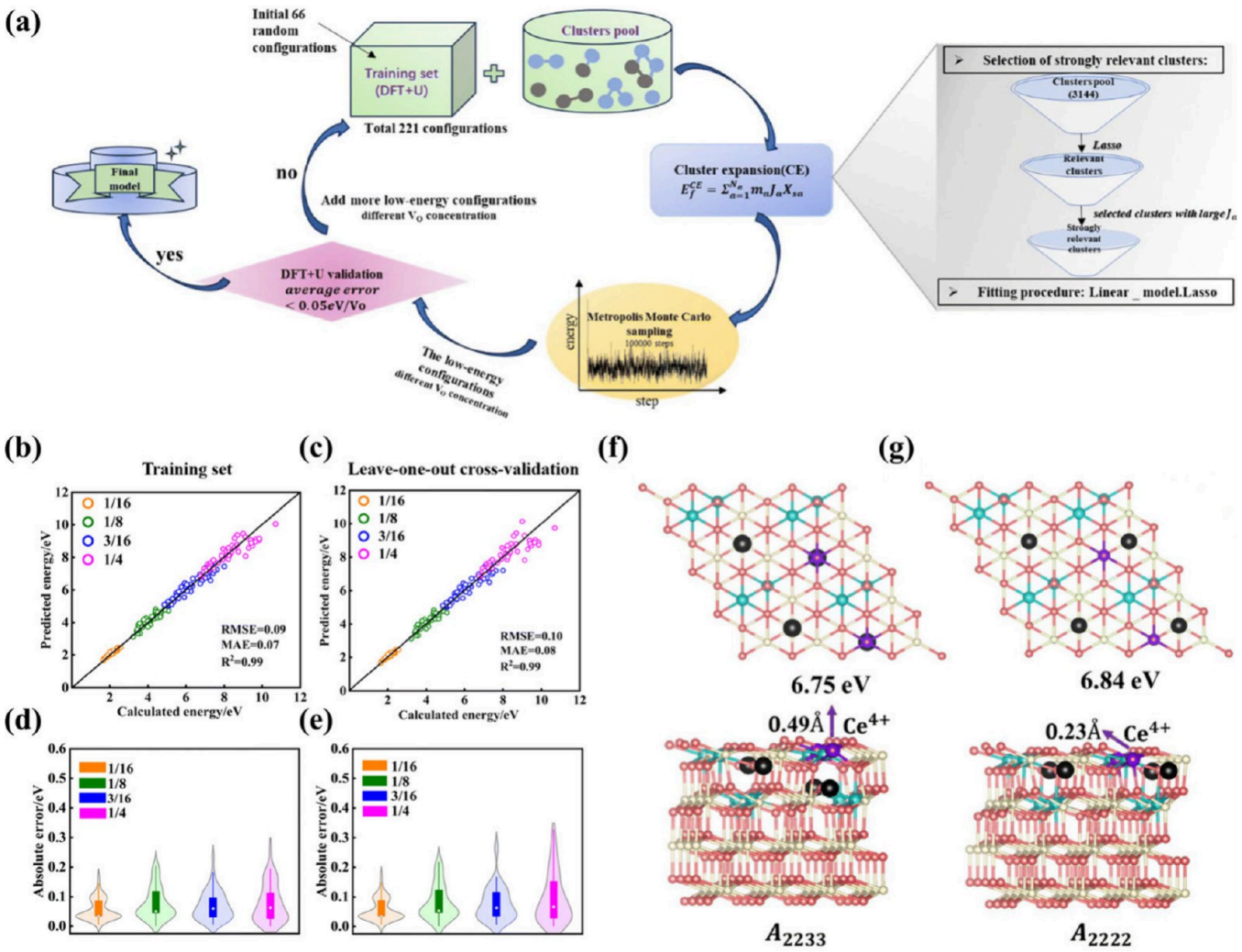

Figure 8. (a) Statistical learning flowchart of the CE model. (b, c) The error between the CE model-predicted energy and the DFT energy for training set (b) and leave-one-out cross-validation (c). (d, e) Violin plots of the absolute error in the energy of configurations for training set (d) and leave-one-out cross-validation (e). (f, g) Top views, side views, and the O vacancy formation energies of the configurations A2233 (with two O vacancies in the subsurface layer and two O vacancies in the third oxygen layer) and A2222 (with four O vacancies in the subsurface layer). Reproduced with permission from ref 84. Copyright 2025 Royal Society of Chemistry.

that mimic or counteract externally applied strain, providing an additional level of control over ceria's surface properties.[114]

To investigate how strain affects the electronic structure of CeO_2 and, in turn, influences the formation energy of surface O_V's, Han and colleagues systematically studied the surface electronic structure and O_V formation energy of $CeO_2(111)$ surfaces under various strain conditions (Figure 12).[117] The study, utilizing spin-polarized DFT+U calculations, systematically analyzed how tensile and compressive strains affect the stability and distribution of O_V's on the $CeO_2(111)$ surface. Their findings highlight that strain not only alters the stability of O_V's but also changes the electronic environment and redistribution of Ce^{3+} polarons. Under tensile strain, the research reveals that surface O_V's are energetically favored due to the stabilization of next-nearest neighbor Ce^{3+} polarons. Conversely, compressive strain promotes the formation of subsurface O_V's, which are associated with nearest neighbor Ce^{3+} polarons. Moreover, the study identifies that compressive strain induces significant changes in defect clustering behavior, making the formation of surface and subsurface O_V dimers more favorable. The authors also found that strain modulates the band gap and defect state positions, providing a direct link between strain engineering and ceria's catalytic performance.

Another effective approach to regulating O_V behavior is through doping. Xu and co-workers systematically investigate the formation of O_V's on transition metal-doped ceria surfaces using a combination of DFT+U calculations and machine learning techniques (Figure 13).[86] The authors focus on uncovering the role of transition metal dopants in modulating O_V formation energy and stability on ceria surfaces. By exploring 97 transition metal-doped ceria systems across various crystallographic facets ($CeO_2(111)$, $CeO_2(110)$, and $CeO_2(100)$), they analyze the correlations between O_V formation energies and the intrinsic properties of dopants, including electronegativity, d-orbital characteristics, and Fermi level (Figure 13a and 13b). Key insights are derived through the application of symbolic regression (SISSO) and subgroup discovery (SGD) methodologies (Figure 13c–f). SISSO identifies low-dimensional descriptors that accurately predict O_V formation energy. Meanwhile, SGD reveals localized patterns within the data set, highlighting the influence of dopant electronegativity, Fermi level, and the p-band center of lattice oxygen. These analyses

https://doi.org/10.1021/jacsau.5c00095
JACS Au 2025, 5, 1549–1569

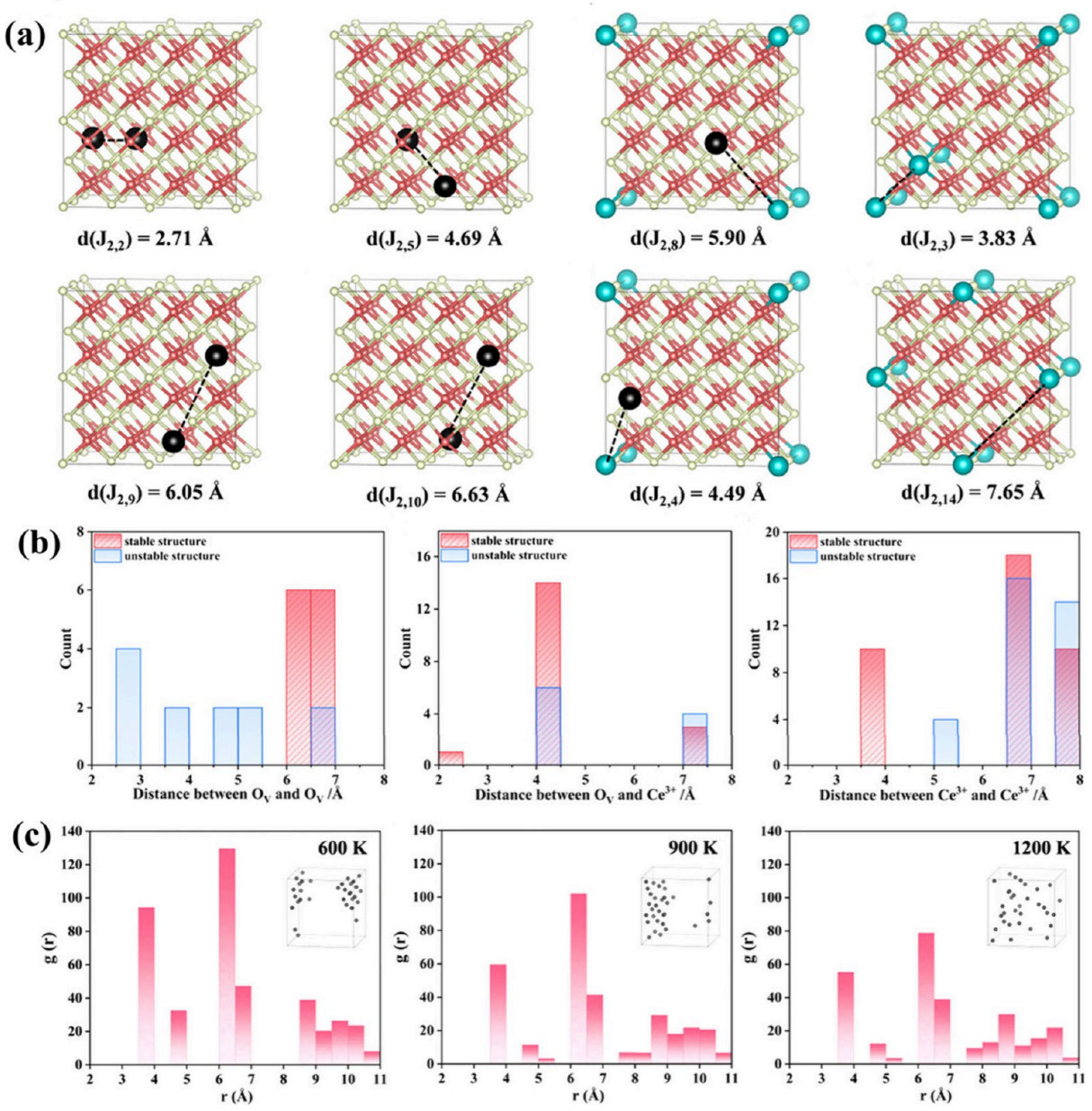

Figure 9. (a) Cluster configurations and distances for two-body interactions with strong repulsive effects: $J_{2,2}$, $J_{2,5}$, $J_{2,8}$, $J_{2,3}$; and strong attractive effects: $J_{2,9}$, $J_{2,10}$, $J_{2,4}$, $J_{2,14}$. Black, white, red, and blue spheres represent oxygen vacancies, Ce^{4+}, O, and Ce^{3+} ions, respectively. (b) Distribution of different distances between vacancies, vacancies and Ce^{3+}, and Ce^{3+} ions in the most stable and unstable configurations of 3 × 3 × 3 supercell with O_V concentration c = 4/216. (c) Statistical average of the radial distribution function of oxygen vacancy at different temperatures with corresponding lattice structure showing oxygen vacancy distribution. Reprinted with permission from ref 85. Copyright 2024 American Chemical Society.

reveal that dopants with higher electronegativity and optimized electronic states near the Fermi level significantly reduce O_V (Figure 13g–i). The study concludes that the interplay of dopant electronic properties and local structural distortions governs O_V behavior.

4. INFLUENCE OF OXYGEN VACANCIES ON THE SURFACE CHEMISTRY OF CERIA

4.1. Surface Reconstructions

O_V's on the CeO_2 surface play a critical role in driving structural reconstructions and altering the material's physical and chemical properties. Surface reconstructions in CeO_2 due to O_V's typically involve lattice distortions and shifts in atomic positions. In particular, the creation of an O_V breaks local Ce–O bonds, causing neighboring Ce atoms to adjust their positions. These adjustments reduce the coordination environment of local Ce cations, which can become Ce^{3+} to compensate for charge imbalance. Consequently, the surface region can exhibit altered stoichiometry, potentially forming facets or adopting new phases that differ from the bulk structure. With increasing vacancy concentration, the reconstruction can become more extensive, leading to rearrangements such as alternating layers of oxygen-deficient and fully oxidized regions, or the formation of extended defects like vacancy clusters.[59,123−126] On a microscopic level, these vacancies can act as trapping sites for adsorbates, facilitating or hindering catalytic reactions depending on the nature of the reactants. This capacity for adapting and reshaping surface structure in response to redox conditions is one of the

https://doi.org/10.1021/jacsau.5c00095
JACS Au 2025, 5, 1549−1569

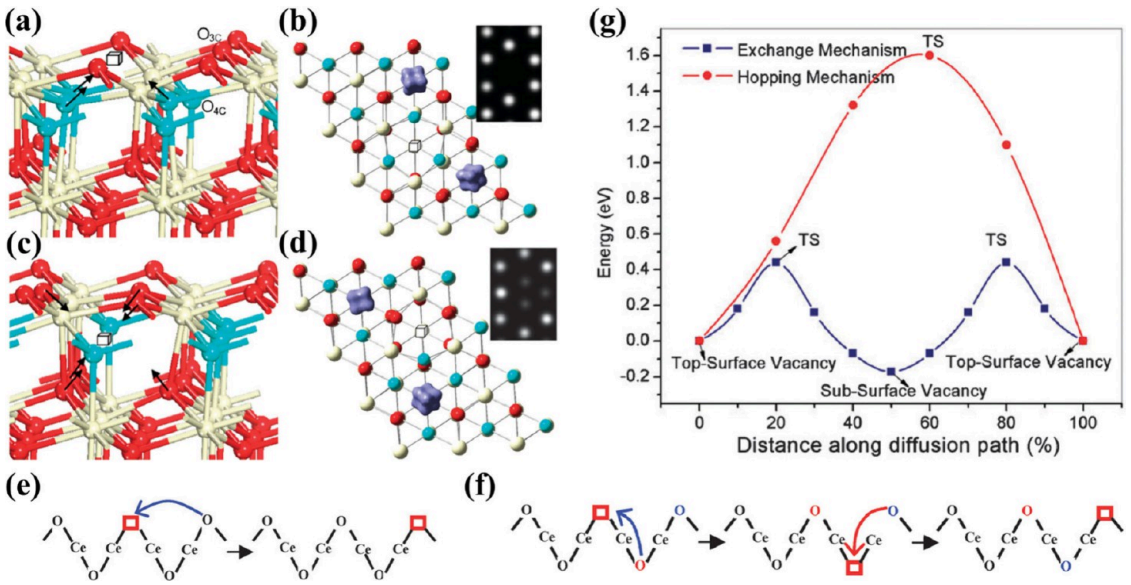

Figure 10. (a–d) The side views and isosurfaces (0.05 e/Å^3) of spin density for CeO_2(111) in the presence of surface (a and b) and subsurface (c and d) oxygen vacancies, respectively. The subsurface O is marked in blue, and other O is in red. Ce is marked in gray. Oxygen vacancies are highlighted in the white boxes. The arrows indicate the directions of atom movements during the structural relaxation. (e) Hopping mechanism. The red boxes show O vacancies. The blue arrow indicates the O diffusion path. (f) Two-step exchange mechanism. The red boxes show O vacancies. The blue and red arrows indicate the O diffusion from the subsurface and surface positions to the O vacancies, respectively. (g) Energy profiles of the hopping and two-step exchange mechanisms. Reproduced with permission from ref 113. Copyright 2011 Royal Society of Chemistry.

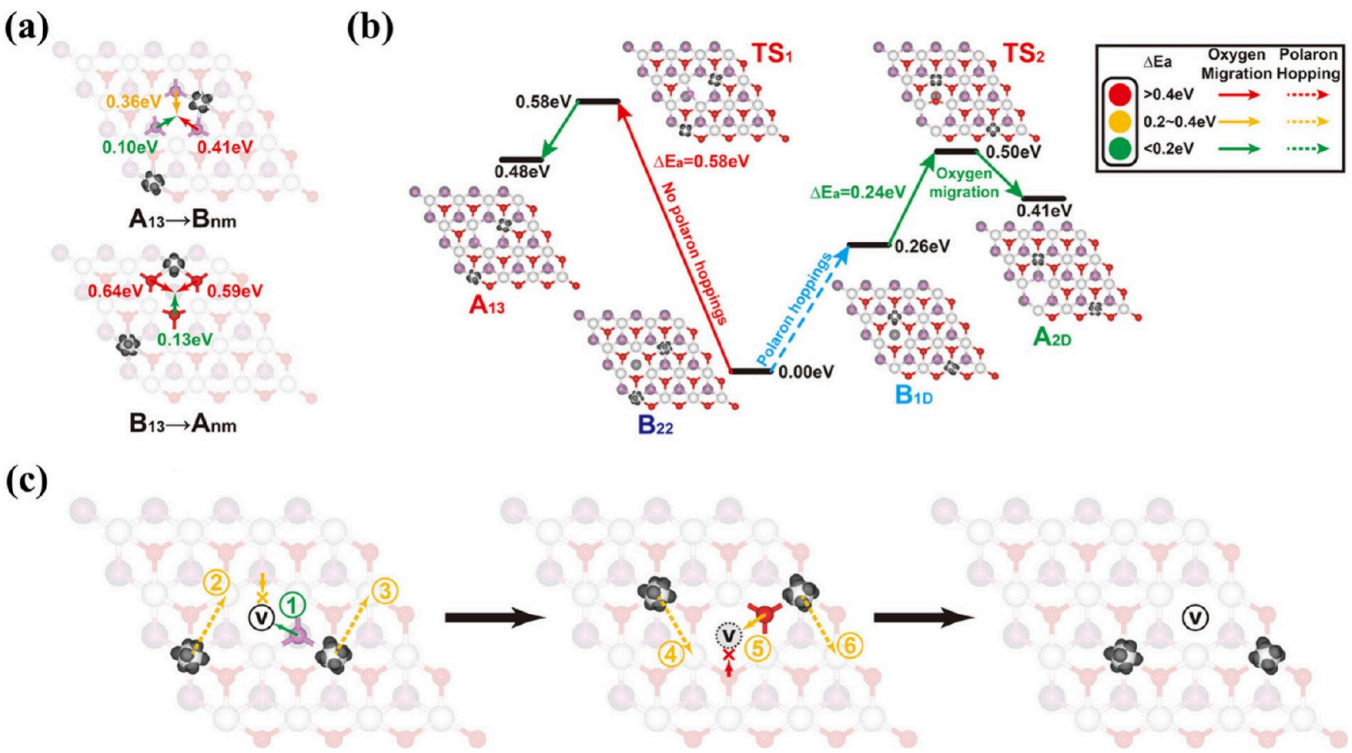

Figure 11. (a, b) Examples of the two oxygen migration mechanisms: (a) the NN-polaron-hindered mechanism; (b) the NN-polaron-promoted mechanism. (c) Schematic view of possible O vacancy migration pathways at the CeO_2(111) surface. "x" here indicates the oxygen migrations that are difficult and thus less likely to occur. Reproduced with permission from ref 34. Copyright 2019 American Physical Society.

core reasons that CeO_2 has found widespread application in catalysis.

The CeO_2(100) surface possesses the highest surface energy, making it most prone to reconstruction. To begin, we will examine whether the CeO_2(100) surface is oxygen-terminated or cerium-terminated. Pan et al. investigate the structural and polarity-compensation mechanisms of ceria nanocrystals exposing the (100) facets.[127] By employing high-resolution STM and DFT+U, the study systematically investigates the atomic configurations of ceria nanocrystals grown on Ru(0001) substrates and annealed under oxygen-deficient conditions. The (100) facets are shown to exhibit two distinct surface

https://doi.org/10.1021/jacsau.5c00095
JACS Au 2025, 5, 1549–1569

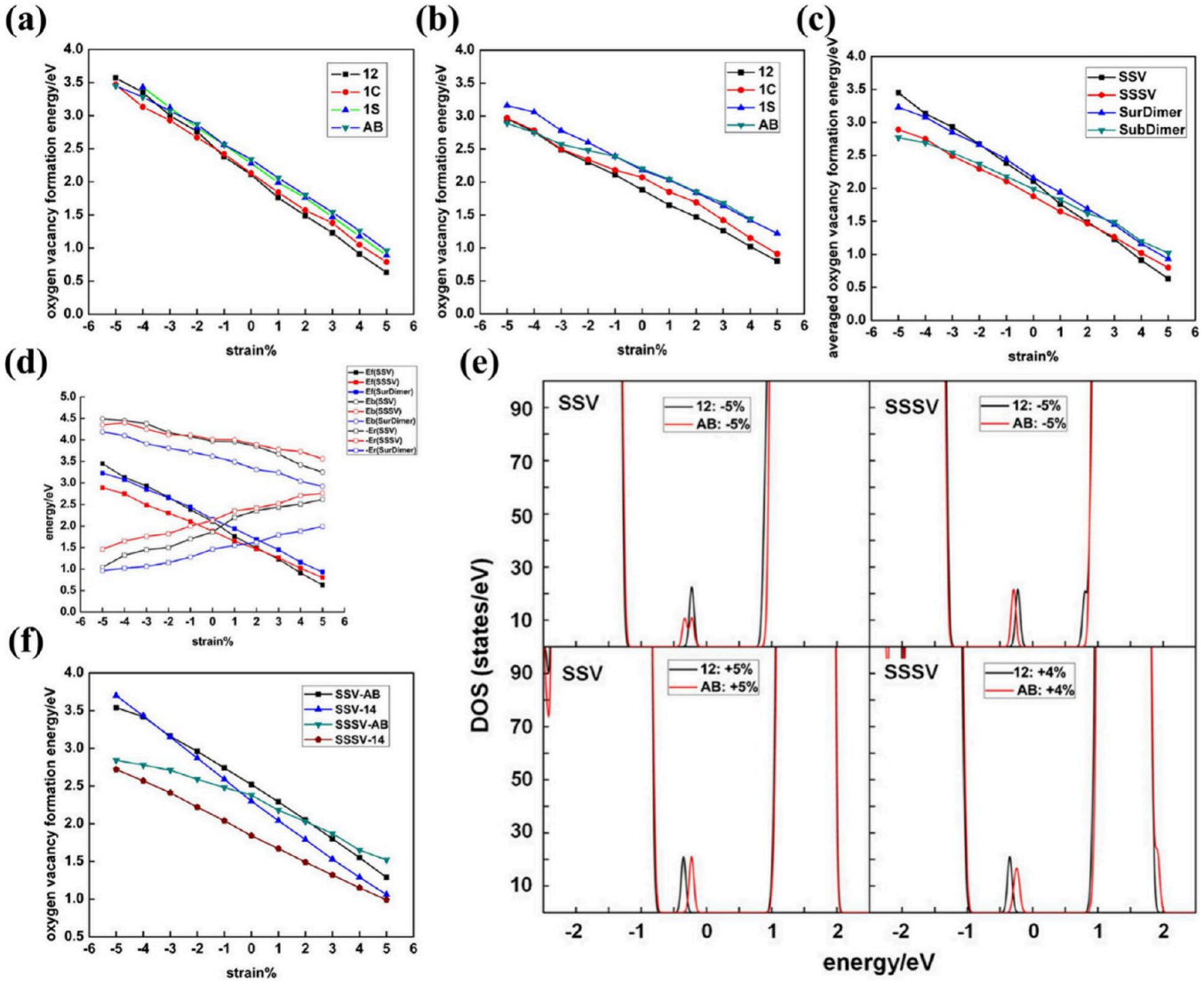

Figure 12. (a, b) Single surface oxygen vacancy (SSV) (a) and single subsurface oxygen vacancy (SSSV) (b) formation energy at the 5 × 5 CeO_2(111) surface as a function of strain and for distinct polaronic structures. (c) The averaged oxygen vacancy formation energy of the most stable SSV, SSSV, SurDimer, and SubDimer structures with 5 × 5 periodicity as a function of strain. (d) The (average) near-surface oxygen vacancy formation energy, $E_f = E_b + E_r$, as a function of strain (5 × 5 periodicity). E_b is the energy cost to create a near-surface oxygen vacancy structure without allowing for lattice relaxations, i.e., the bond breaking energy, and E_r, the energy gained from lattice relaxations in the presence of the vacancies. (e) Densities of states (DOS) summed over spin projections and all atoms for a SSV and SSSV under −5%, and +5%, or +4% strain with AB and 12 Ce^{3+} configurations and 5 × 5 periodicity. Nearest (NN) and next-nearest neighbor (NNN) Ce ions to vacancies are labeled with uppercase letters (A, B, C, D, ...) and numerals (1, 2, 3, 4, ...), respectively. The Fermi level is set as the zero energy value, below which the states are occupied. (f) Oxygen vacancy formation energy for single surface (SSV) and subsurface (SSSV) vacancies at the 2 × 2 CeO_2(111) surface as a function of strain and for distinct polaronic structures. Reproduced from ref 117. Available under a CC BY 4.0 license.

reconstructions, (2 × 2) and c(2 × 2), that effectively compensate for the intrinsic dipole of the polar (100) plane. The authors reveal that the primary (2 × 2) reconstruction consists of pyramidal CeO_4 units similar to the Wulff reconstruction, while the c(2 × 2) phase involves a checkerboard-like O_V pattern. These configurations stabilize the (100) facets against polarity-induced instability, enabling their experimental observation. The study also identifies the influence of O_V's in reducing the ceria lattice, which contributes to the evolution of the crystal shape under high-temperature annealing. The work by Capdevila-Cortada and co-workers focus on elucidating the role of configurational entropy in stabilizing the polar CeO_2(100) surface.[128] By combining DFT+U calculations with molecular dynamics simulations, the authors systematically analyze the structural and energetic characteristics of different surface terminations. They identify the CeO_4-t and O-t reconstructions as the most relevant configurations and demonstrate that their stability is influenced not only by surface energy but also by entropy contributions. The study highlights the critical role of configurational entropy, derived from the degeneracy of surface oxygen distributions, in enhancing the stability of polar surfaces, particularly at elevated temperatures. Furthermore, the simulations reveal facile oxygen diffusion processes on the O-t surface, suggesting dynamic behavior that further supports configurational entropy's stabilizing effects. The work highlights the importance of entropy in explaining the coexistence of multiple reconstructions and their temperature-dependent transformations.

https://doi.org/10.1021/jacsau.5c00095
JACS Au 2025, 5, 1549−1569

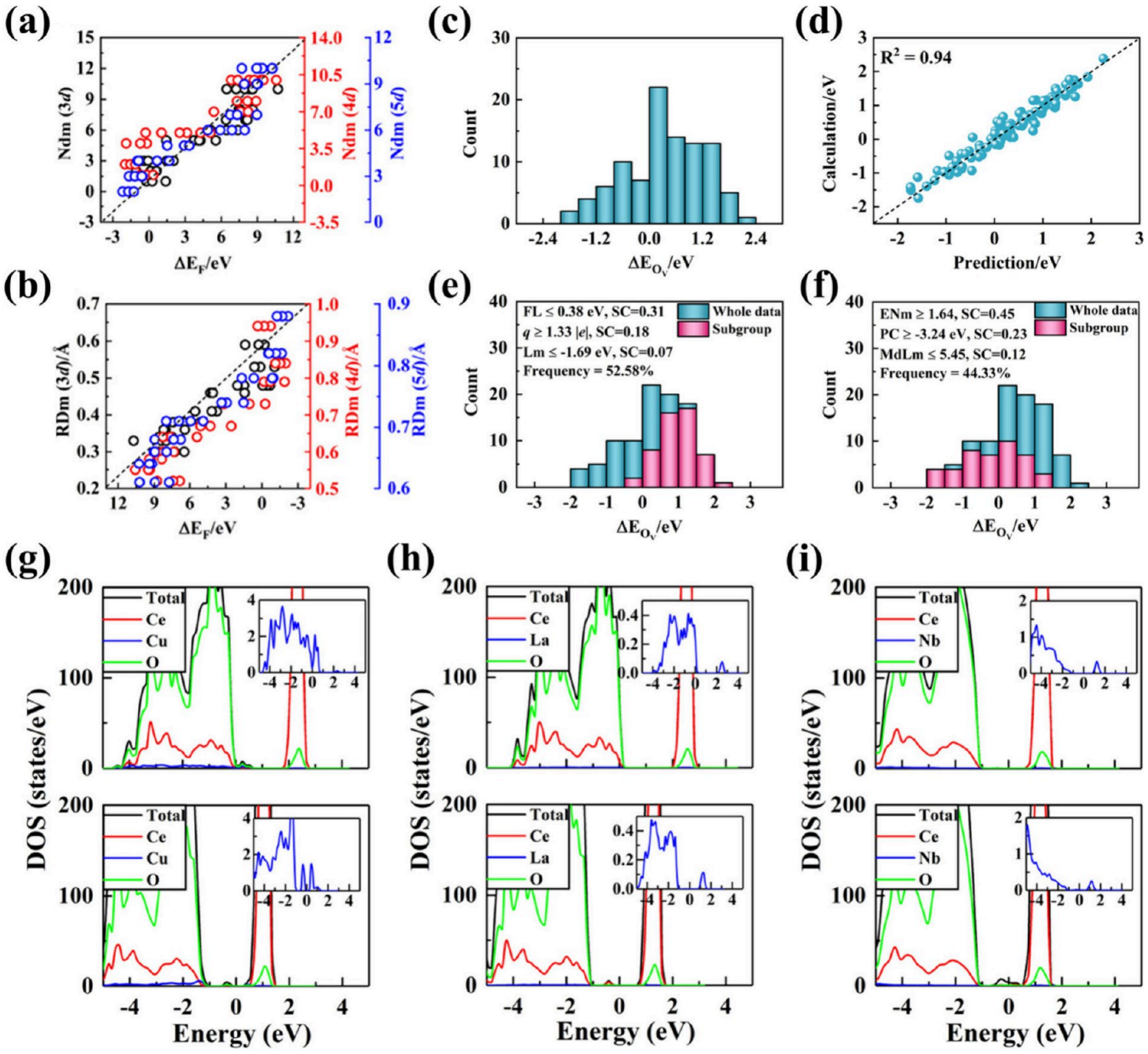

Figure 13. (a) The correlation between the formation energies (ΔE_F) of TM-doped ceria systems and Ndm. (b) The correlation between ΔE_F and RDm. (c) The histogram distribution of data samples for O_V formation energies of the TM-doped ceria systems, (d) the error distribution between the SISSO model predicted energies and DFT calculated energies for the TM-doped ceria systems, and the results of the SGD by maximizing (e) and minimizing (f) the surface O_V formation energies. (g–i) Species projected density of states for surface doped $CeO_2(111)$ surfaces. The TM-doped $CeO_2(111)$ surfaces with low O_V formation energy (g, Cu doping), moderate O_V formation energy (h, La doping), and high O_V formation energy (i, Nb doping). Reproduced with permission from ref 86. Copyright 2024 Royal Society of Chemistry.

These studies demonstrate that O_V's have a significant impact on the surface structure of $CeO_2(100)$. To uncover new surface reconstructions, it is essential to systematically investigate the O_V configurations under varying oxygen partial pressures. Zhang et al. investigated the intricate reconstruction of the polar $CeO_2(100)$ surface under conditions of high reduction and elevated temperatures, addressing its structural complexity and catalytic significance (Figure 14).[68] By employing in situ spherical aberration-corrected scanning transmission electron microscopy (STEM) and particle swarm optimization (PSO) algorithms, the authors identified a (4 × 6) surface reconstruction (Figure 14a and 14b). This unique reconstruction features Ce_3O_X chains, where Ce and O atoms organize into a stable periodic structure. The reconstructed surface arises under highly reducing environments and high-temperature conditions, demonstrating significant structural adaptation (Figure 14c). DFT+U calculations provided further insights into the stability mechanisms of the reconstructed surface, highlighting strong hybridization between Ce(4f) and O(2p) orbitals (Figure 14j). This electronic interaction plays a critical role in stabilizing the surface structure and enhancing its chemisorption properties.

4.2. Supported Metal Catalysts

CeO_2 is a popular support material for metal catalysts due to its unique ability to form and heal O_V. These vacancies are more than simple defects, they change the way electrons move on and around the surface, which can greatly affect how metal particles

https://doi.org/10.1021/jacsau.5c00095
JACS Au 2025, 5, 1549–1569

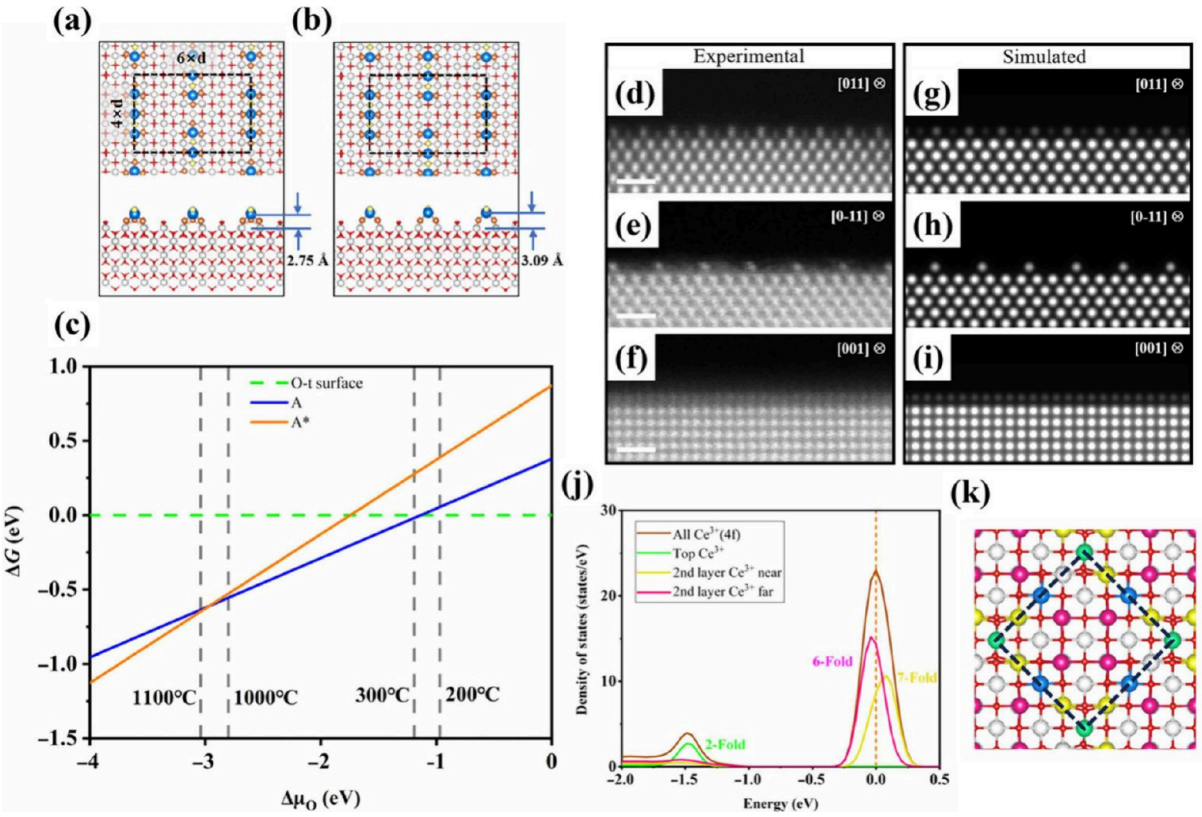

Figure 14. (a, b) Top view and side view of $CeO_2(100)$-(4×6)-A (a) and $CeO_2(100)$-(4×6)-A* (b), respectively, where white balls represent bulk Ce atoms, red balls represent bulk O atoms, blue balls represent surface Ce atoms, yellow balls represent O atoms at the apex of the Ce_3O_x chains, and orange balls represent surface O atoms beside the Ce_3O_x chains. Black dashed lines indicate the surface reconstruction period. (c) The stability of structures with different compositions is depicted as a function of oxygen chemical potential $\Delta\mu O$. The simulated environmental oxygen partial pressure is 2.0×10^{-8} mbar. (d–i) Experimental measured (d–f) and theoretically simulated (g–i) HAADF STEM images of the reconstructed $CeO_2(100)$ surface along different zone axes. (j, k) $Ce^{3+}(4f)$ projected on different sets of Ce^{3+} cations for structure B (j), with reference to the color of the atoms in (k) for structure B. Reproduced with permission from ref 68. Copyright 2024 American Association for the Advancement of Science.

attach to the support.[129−134] In many catalytic systems, this interaction is key to controlling how well the catalyst performs. One reason these vacancies are so important is that they allow cerium ions in the oxide lattice to switch between two oxidation states: Ce^{4+} and Ce^{3+}. When an oxygen atom is removed, nearby Ce^{4+} ions can gain an electron and change into Ce^{3+}. This shift can alter the local electronic environment on the surface and provide extra sites for metal atoms to anchor. As a result, the metal particles, which could be platinum, palladium, gold, or other metals, bond more tightly to the oxide. This reduces the chance that the metal particles will sinter at high temperatures, which can keep the catalyst active for a longer time. O_V's also help improve the catalyst's performance by acting as active sites for different reaction steps.

Han et al. systematically investigated the interaction between gold clusters and $CeO_2(111)$ surfaces, with a particular emphasis on the structural evolution of Au clusters on reduced $CeO_2(111)$ surfaces and its implications for catalytic behavior.[135] Using DFT+U, the authors systematically investigated how different types of O_V structures on ceria, including single surface vacancies (SSV), linear surface vacancy trimers (LSVT), double linear vacancy clusters (dLSVC), and triangular surface vacancy trimers (TSVT), influence the stability, morphology, and electronic properties of Au clusters. They found that O_V's act as nucleation sites for Au clusters, with stronger binding energies compared to clean surface sites. The study revealed that Au clusters transition from 2D to 3D structures depending on the vacancy type and cluster size. Notably, the transition size increases in the order TSVT > dLSVC ~ LSVT > SSV, driven by charge transfer between the Au clusters and ceria surface.

Under realistic reaction conditions, catalysts are often dynamic, with both their surface geometric structures and electronic structures undergoing corresponding changes. Zhang and co-workers studied the fluxionality of electronic structures in supported Pd clusters on a CeO_2 substrate under reaction conditions.[83] The authors employed ab initio molecular dynamics simulations and DFT+U to reveal the dynamic interactions between the metal clusters and the ceria surface. A key finding of the research is that the electronic configurations of both the Pd clusters and the ceria substrate exhibit significant fluctuations during the catalytic process. These fluctuations are closely tied to structural distortions in the Pd clusters and their interaction with the CeO_2 surface, which is characterized by strong Pd−O bonding and variations in Ce^{3+}/Ce^{4+} distributions. The study also highlights that these dynamic electronic and structural changes significantly influence the catalytic activity of the Pd clusters. Variations in charge distribution, magnetic moments, and density of states were observed, emphasizing the critical role of these electronic changes in controlling catalytic behavior. The authors further demonstrated how these effects impact the adsorption energies of small molecules such as CO and NO, showcasing that charge redistribution in the Pd clusters can alter their binding strength and reaction pathways. The findings highlight the importance of considering dynamic

https://doi.org/10.1021/jacsau.5c00095
JACS Au 2025, 5, 1549−1569

electronic configurations to accurately evaluate the activity of supported metal catalysts, particularly under high-temperature reaction conditions. This work provides a deeper understanding of metal−support interactions.

5. CHALLENGES IN UNDERSTANDING OXYGEN VACANCIES

Understanding surface O_V's on ceria presents significant challenges due to the intricate interactions between vacancies and Ce^{3+} ions, as well as the resulting multiconfigurational distributions. O_V's are inherently linked to the reduction of Ce^{4+} to Ce^{3+}, a process that introduces a wide variety of possible spatial and electronic configurations. These configurations are highly sensitive to external variables such as temperature, oxygen partial pressure, and the presence of adsorbates, making them highly dynamic. The spatial localization of Ce^{3+} ions around O_V's induces geometric distortions and electronic changes in the ceria lattice. These localized Ce^{3+} ions interact with the surrounding lattice, creating a network of complex interactions that are not easily captured using traditional computational or experimental methods. Moreover, these interactions often lead to the formation of clusters or patterns that are difficult to predict or validate, further complicating the understanding of ceria's defect chemistry.

The dynamic interplay between O_V's and Ce^{3+} ions creates a landscape of configurational diversity that is both complex and multifaceted. Multiple vacancy configurations coexist, each influenced by factors such as the coupling between Ce^{3+} ions, which can exhibit long-range interactions across the lattice. This configurational diversity is amplified by temperature-dependent behavior and catalytic environments, where vacancy structures dynamically evolve to adapt to reaction conditions. The presence of long-range Ce^{3+}-Ce^{3+} coupling introduces additional layers of complexity, creating a rich, multibody interaction framework that governs ceria's catalytic and functional properties. These dynamic interactions challenge conventional theoretical models, necessitating advanced methodologies like multiscale simulations and machine learning to adequately describe these phenomena.

Additionally, the distribution of O_V's and their interactions with Ce^{3+} ions are far from static. Under catalytic or high-temperature conditions, these distributions exhibit fluxional behavior, dynamically evolving in response to reaction environments or applied stresses. This fluxionality complicates efforts to determine the dominant structural motifs and their associated mechanistic roles. Experimental techniques, such as in situ spectroscopy and microscopy, provide snapshots of these dynamic systems but often lack the temporal resolution to fully capture the real-time evolution of vacancy configurations. Computational approaches, including cluster expansion models and high-throughput simulations, are essential for mapping the configurational space, but their accuracy heavily depends on the inclusion of multibody interactions and dynamic effects. Solving these challenges is critical, as the interplay between O_V's and Ce^{3+} ions directly impacts ceria's oxygen mobility, redox properties, and catalytic efficiency, underscoring the importance of integrating advanced theoretical and experimental tools to unlock the full potential of ceria-based materials.

6. FUTURE DIRECTIONS

Future research on ceria surface O_V's will greatly benefit from the integration of multiscale modeling techniques. O_V's and their interactions with Ce^{3+} ions involve complex phenomena that span different time and length scales. Atomic-scale mechanisms, such as the creation, migration, and clustering of vacancies, are best captured by quantum mechanical methods like DFT. However, these approaches often struggle to account for long-range interactions or collective behaviors, such as the cooperative dynamics of vacancy networks or the impact of environmental conditions like temperature and pressure. Multiscale modeling bridges this gap by linking atomistic models with mesoscale and continuum methods, enabling the study of system-wide behaviors while retaining atomic-level accuracy. Techniques like kinetic Monte Carlo simulations, cluster expansion models, and molecular dynamics can simulate the dynamic evolution of O_V's under catalytic conditions. These methods allow researchers to explore how vacancies influence large-scale properties such as oxygen transport, surface reconstruction, and catalytic activity. Combining multiscale models with experimental data can provide a more holistic understanding, ultimately leading to predictive models for ceria's performance under various operating conditions.

The application of artificial intelligence (AI) in studying O_V's on ceria surfaces offers an unprecedented opportunity to accelerate discovery and improve predictive capabilities. Machine learning (ML) algorithms can analyze vast amounts of data generated from first-principles calculations, high-throughput simulations, and experimental results, identifying patterns and uncovering hidden relationships between structural, electronic, and catalytic properties. AI-driven methods, such as subgroup discovery and gradient boosting regression, can pinpoint key descriptors like vacancy formation energies, d-band centers, and Ce^{3+}-vacancy coupling, which are critical for predicting material performance. Furthermore, reinforcement learning can be used to explore optimal configurations of vacancies and dopants, offering pathways to enhance ceria's catalytic properties. The development of AI-driven models that integrate multiple data sources, ranging from in situ experimental data to computational predictions, will enable real-time analysis of ceria's dynamic behavior under reaction conditions. These advancements will also support the design of tailored ceria-based catalysts, optimizing properties such as oxygen mobility and redox efficiency for specific applications like fuel cells and environmental remediation.

To fully understand and harness the role of O_V's on ceria surfaces, future research must emphasize the integration of experimental and theoretical approaches. Advanced experimental techniques, such as in situ scanning transmission electron microscopy (STEM), X-ray absorption spectroscopy (XAS), and surface-enhanced infrared absorption spectroscopy (SEIRAS), provide invaluable insights into the dynamic behavior of vacancies under real reaction conditions. However, these methods often lack the temporal or spatial resolution to capture fast processes or localized interactions. Theoretical methods, including DFT and cluster expansion models, can fill these gaps by offering detailed atomic-scale insights. The combination of these two approaches enables a synergistic understanding of ceria's behavior: experimental results can validate and refine theoretical predictions, while simulations can guide the design of targeted experiments. Moreover, advances in operando techniques, capable of capturing real-time changes in surface structure and electronic properties, can be paired with high-throughput computational workflows to explore a wide range of reaction conditions. This combined strategy ensures a comprehensive understanding of O_V behavior, paving the way

https://doi.org/10.1021/jacsau.5c00095
JACS Au 2025, 5, 1549−1569

for the development of next-generation ceria-based materials with optimized catalytic and functional properties.

7. CONCLUSIONS

In conclusion, O_V's play a critical role in defining the electronic structure, catalytic activity, and oxygen storage capability of ceria. These defects are not static but dynamically interact with Ce^{3+} ions, leading to complex structural and electronic rearrangements that significantly influence ceria's surface chemistry. The diversity in O_V configurations, driven by polaron formation and lattice distortions, introduces unique challenges in understanding their role, particularly under operational conditions where external factors such as temperature, oxygen partial pressure, and dopants further complicate their behavior. Computational approaches, including density functional theory (DFT) with hybrid functionals and Hubbard corrections (DFT +U), have provided valuable insights into the mechanisms of O_V formation, clustering, and migration, offering a pathway to rationalize experimental observations from techniques such as STM and DFM. Despite these advances, challenges remain, particularly in accurately capturing the multiconfigurational nature of O_V interactions and their dynamic evolution in response to environmental changes. Future research must prioritize multiscale modeling to bridge the gap between atomic-level simulations and macroscopic behavior, enabling a more comprehensive understanding of O_V dynamics. The integration of AI-driven discovery methods offers promising opportunities to efficiently explore the vast configuration space of O_V's, identify key descriptors, and predict catalytic behavior with high accuracy. Additionally, combining experimental techniques with theoretical frameworks will be critical in validating computational predictions and unveiling real-time O_V dynamics under operating conditions.

AUTHOR INFORMATION

Corresponding Author

Yi Gao − *Photon Science Research Center for Carbon Dioxide, Shanghai Advanced Research Institute, Chinese Academy of Sciences, Shanghai 201210, China; State Key Laboratory of Low Carbon Catalysis and Carbon Dioxide Utilization, Shanghai Advanced Research Institute, Chinese Academy of Sciences, Shanghai 201210, China;* orcid.org/0000-0001-6015-5694; Email: gaoyi@sari.ac.cn

Authors

Zhong-Kang Han − *School of Materials Science and Engineering, Zhejiang University, Hangzhou 310027, China;* orcid.org/0000-0003-1489-6824

Wen Liu − *School of Materials Science and Engineering, Zhejiang University, Hangzhou 310027, China*

Complete contact information is available at: https://pubs.acs.org/10.1021/jacsau.5c00095

Author Contributions

The manuscript was written through contributions of all authors.

Notes

The authors declare no competing financial interest.

ACKNOWLEDGMENTS

This project was supported by the National Key R&D Program of China (2023YFA1506900, 2022YFA1505500), the National Natural Science Foundation of China (12174408, 22302173), the Natural Science Foundation of Shanghai (22JC1404200), and the Foundation of Key Laboratory of Low-Carbon Conversion Science & Engineering, Shanghai Advanced Research Institute, Chinese Academy of Sciences (KLLCCSE-202201Z, SARI, CAS).

REFERENCES

(1) Nolan, M.; Fearon, J. E.; Watson, G. W. Oxygen Vacancy Formation and Migration in Ceria. *Solid State Ion.* **2006**, *177* (35), 3069−3074.

(2) Nolan, M.; Parker, S. C.; Watson, G. W. The Electronic Structure of Oxygen Vacancy Defects at the Low Index Surfaces of Ceria. *Surf. Sci.* **2005**, *595* (1), 223−232.

(3) Zhang, C. J.; Michaelides, A.; King, D. A.; Jenkins, S. J. Oxygen Vacancy Clusters on Ceria: Decisive Role of Cerium f Electrons. *Phys. Rev. B* **2009**, *79* (7), No. 075433.

(4) Castleton, C. W. M.; Kullgren, J.; Hermansson, K. Tuning LDA+U for Electron Localization and Structure at Oxygen Vacancies in Ceria. *J. Chem. Phys.* **2007**, *127* (24), No. 244704.

(5) Gopal, C. B.; Van de Walle, A. Ab Initio Thermodynamics of Intrinsic Oxygen Vacancies in Ceria. *Phys. Rev. B* **2012**, *86* (13), No. 134117.

(6) Choudhury, B.; Choudhury, A. Ce^{3+} and Oxygen Vacancy Mediated Tuning of Structural and Optical Properties of CeO_2 Nanoparticles. *Mater. Chem. Phys.* **2012**, *131* (3), 666−671.

(7) Paier, J.; Penschke, C.; Sauer, J. Oxygen Defects and Surface Chemistry of Ceria: Quantum Chemical Studies Compared to Experiment. *Chem. Rev.* **2013**, *113* (6), 3949−3985.

(8) Mamontov, E.; Egami, T.; Brezny, R.; Koranne, M.; Tyagi, S. Lattice Defects and Oxygen Storage Capacity of Nanocrystalline Ceria and Ceria-Zirconia. *J. Phys. Chem. B* **2000**, *104* (47), 11110−11116.

(9) Murgida, G. E.; Ferrari, V.; Ganduglia-Pirovano, M. V.; Llois, A. M. Ordering of Oxygen Vacancies and Excess Charge Localization in Bulk Ceria: A DFT Plus U Study. *Phys. Rev. B* **2014**, *90* (11), No. 115120.

(10) Dutta, P.; Pal, S.; Seehra, M. S.; Shi, Y.; Eyring, E. M.; Ernst, R. D. Concentration of Ce^{3+} and Oxygen Vacancies in Cerium Oxide Nanoparticles. *Chem. Mater.* **2006**, *18* (21), 5144−5146.

(11) Liu, Y.; Wen, C.; Guo, Y.; Lu, G. Z.; Wang, Y. Q. Effects of Surface Area and Oxygen Vacancies on Ceria in CO Oxidation: Differences and Relationships. *J. Mole. Catal. A-Chem.* **2010**, *316* (1), 59−64.

(12) Kim, H. J.; Jang, M. G.; Shin, D.; Han, J. W. Design of Ceria Catalysts for Low-Temperature CO Oxidation. *ChemCatChem.* **2020**, *12* (1), 11−26.

(13) Davó-Quiñonero, A.; Bailón-García, E.; López-Rodríguez, S.; Juan-Juan, J.; Lozano-Castelló, D.; García-Melchor, M.; Herrera, F. C.; Pellegrin, E.; Escudero, C.; Bueno-López, A. Insights into the Oxygen Vacancy Filling Mechanism in CuO/CeO_2 Catalysts: A Key Step toward High Selectivity in Preferential CO Oxidation. *ACS Catal.* **2020**, *10* (11), 6532−6545.

(14) Laguna, O. H.; Pérez, A.; Centeno, M. A.; Odriozola, J. A. Synergy between Gold and Oxygen Vacancies in Gold Supported on Zr-Doped Ceria Catalysts for the CO Oxidation. *Appl. Catal. B: Environ.* **2015**, *176*, 385−395.

(15) Widmann, D.; Leppelt, R.; Behm, R. J. Activation of a Au/CeO_2 Catalyst for the CO Oxidation Reaction by Surface Oxygen Removal/Oxygen Vacancy Formation. *J. Catal.* **2007**, *251* (2), 437−442.

(16) Sayle, T. X. T.; Parker, S. C.; Catlow, C. R. A. The Role of Oxygen Vacancies on Ceria Surfaces in the Oxidation of Carbon-Monoxide. *Surf. Sci.* **1994**, *316* (3), 329−336.

(17) Lykaki, M.; Pachatouridou, E.; Carabineiro, S. A. C.; Iliopoulou, E.; Andriopoulou, C.; Kallithrakas-Kontos, N.; Boghosian, S.;

Konsolakis, M. Ceria Nanoparticles Shape Effects on the Structural Defects and Surface Chemistry: Implications in CO Oxidation by Cu/CeO_2 Catalysts. *Appl. Catal. B: Environ.* **2018**, *230*, 18−28.
(18) Vecchietti, J.; Bonivardi, A.; Xu, W. Q.; Stacchiola, D.; Delgado, J. J.; Calatayud, M.; Collins, S. E. Understanding the Role of Oxygen Vacancies in the Water Gas Shift Reaction on Ceria-Supported Platinum Catalysts. *ACS Catal.* **2014**, *4* (6), 2088−2096.
(19) Wang, X. Q.; Rodriguez, J. A.; Hanson, J. C.; Gamarra, D.; Martínez-Arias, A.; Fernández-García, M. In Situ Studies of the Active Sites for the Water Gas Shift Reaction over Cu-CeO_2 Catalysts: Complex Interaction between Metallic Copper and Oxygen Vacancies of Ceria. *J. Phys. Chem. B* **2006**, *110* (1), 428−434.
(20) Li, L.; Zhan, Y. Y.; Zheng, Q.; Zheng, Y. H.; Chen, C. Q.; She, Y. S.; Lin, X. Y.; Wei, K. M. Water-Gas Shift Reaction over CuO/CeO_2 Catalysts: Effect of the Thermal Stability and Oxygen Vacancies of CeO_2 Supports Previously Prepared by Different Methods. *Catal. Lett.* **2009**, *130* (3−4), 532−540.
(21) Cao, F. X.; Xiao, Y. S.; Zhang, Z. M.; Li, J.; Xia, Z. M.; Hu, X.; Ma, Y. Y.; Qu, Y. Q. Influence of Oxygen Vacancies of CeO_2 on Reverse Water Gas Shift Reaction. *J. Catal.* **2022**, *414*, 25−32.
(22) Duarte de Farias, A. M.; Nguyen-Thanh, D.; Fraga, M. A. Discussing the Use of Modified Ceria as Support for Pt Catalysts on Water-Gas Shift Reaction. *Appl. Catal. B: Environ.* **2010**, *93* (3), 250−258.
(23) Schilling, C.; Hess, C. Elucidating the Role of Support Oxygen in the Water-Gas Shift Reaction over Ceria-Supported Gold Catalysts Using Operando Spectroscopy. *ACS Catal.* **2019**, *9* (2), 1159−1171.
(24) Liu, H. X.; Li, S. Q.; Wang, W. W.; Yu, W. Z.; Zhang, W. J.; Ma, C.; Jia, C. J. Partially Sintered Copper-Ceria as Excellent Catalyst for the High-Temperature Reverse Water Gas Shift Reaction. *Nat. Commun.* **2022**, *13* (1), 867.
(25) Fu, X.-P.; Guo, L.-W.; Wang, W.-W.; Ma, C.; Jia, C.-J.; Wu, K.; Si, R.; Sun, L.-D.; Yan, C.-H. Direct Identification of Active Surface Species for the Water-Gas Shift Reaction on a Gold-Ceria Catalyst. *J. Am. Chem. Soc.* **2019**, *141* (11), 4613−4623.
(26) Li, Z. R.; Chen, L.; Wu, Z. F.; Jia, A. P.; Shi, S. C.; Zhang, H.; Wang, J.; Liu, Z.; Shao, W. P.; Yang, F.; Wu, X. P.; Gong, X. Q.; Huang, W. X. Surface Oxygen Vacancy and Hydride Species on Ceria Are Detrimental to Acetylene Semihydrogenation Reaction. *ACS Catal.* **2023**, *13* (8), 5213−5224.
(27) Zhao, Y. X.; Jalal, A.; Uzun, A. Interplay between Copper Nanoparticle Size and Oxygen Vacancy on Mg-Doped Ceria Controls Partial Hydrogenation Performance and Stability. *ACS Catal.* **2021**, *11* (13), 8116−8131.
(28) Zhou, Z. Y.; Chen, L.; Wang, L. Y.; Liu, Y.; Cheng, P. H.; Peng, H. R.; Cai, J.; Zhou, Q.; Wang, Y. F.; Yang, N.; Wang, B. B.; Gong, X. Q.; Yang, F.; Liu, Z. Selective Hydrogenation of Propyne to Propene Promoted by Synergistic Effect of Surface Oxygen Vacancies and Hydride Species on Ceria. *ACS Catal.* **2023**, *13* (14), 9588−9596.
(29) Yuan, Z. L.; Huang, L.; Liu, Y. S.; Sun, Y.; Wang, G. H.; Li, X.; Lercher, J. A.; Zhang, Z. H. Synergy of Oxygen Vacancies and Base Sites for Transfer Hydrogenation of Nitroarenes on Ceria Nanorods. *Angew. Chem., Int. Ed.* **2024**, *63* (9), No. e202317339.
(30) Vilé, G.; Bridier, B.; Wichert, J.; Pérez-Ramírez, J. Ceria in Hydrogenation Catalysis: High Selectivity in the Conversion of Alkynes to Olefins. *Angew. Chem., Int. Ed.* **2012**, *51* (34), 8620−8623.
(31) Werner, K.; Weng, X. F.; Calaza, F.; Sterrer, M.; Kropp, T.; Paier, J.; Sauer, J.; Wilde, M.; Fukutani, K.; Shaikhutdinov, S.; Freund, H. J. Toward an Understanding of Selective Alkyne Hydrogenation on Ceria: On the Impact of O Vacancies on H_2 Interaction with CeO_2(111). *J. Am. Chem. Soc.* **2017**, *139* (48), 17608−17616.
(32) Zhang, Z. H.; Wang, Z. Q.; Li, Z. R.; Zheng, W. B.; Fan, L. P.; Zhang, J.; Hu, Y. M.; Luo, M. F.; Wu, X. P.; Gong, X. Q.; Huang, W. X.; Lu, J. Q. Metal-Free Ceria Catalysis for Selective Hydrogenation of Crotonaldehyde. *ACS Catal.* **2020**, *10* (24), 14560−14566.
(33) Singh, R.; Pandey, V.; Pant, K. K. Promotional Role of Oxygen Vacancy Defects and Cu-Ce Interfacial Sites on the Activity of Cu/CeO_2 Catalyst for CO_2 Hydrogenation to Methanol. *ChemCatChem.* **2022**, *14* (24), e202201053.
(34) Zhang, D. W.; Han, Z. K.; Murgida, G. E.; Ganduglia-Pirovano, M. V.; Gao, Y. Oxygen-Vacancy Dynamics and Entanglement with Polaron Hopping at the Reduced CeO_2(111) Surface. *Phys. Rev. Lett.* **2019**, *122* (9), No. 096101.
(35) Wang, Y. G.; Mei, D. H.; Li, J.; Rousseau, R. DFT+U Study on the Localized Electronic States and Their Potential Role During H_2O Dissociation and CO Oxidation Processes on CeO_2(111) Surface. *J. Phys. Chem. C* **2013**, *117* (44), 23082−23089.
(36) Han, Z. K.; Gao, Y. Water Adsorption and Dissociation on Ceria-Supported Single-Atom Catalysts: A First-Principles DFT Plus U Investigation. *Chem.—Eur. J.* **2016**, *22* (6), 2092−2099.
(37) Warren, K. J.; Scheffe, J. R. Role of Surface Oxygen Vacancy Concentration on the Dissociation of Methane over Nonstoichiometric Ceria. *J. Phys. Chem. C* **2019**, *123* (21), 13208−13218.
(38) Trogadas, P.; Parrondo, J.; Ramani, V. CeO_2 Surface Oxygen Vacancy Concentration Governs in Situ Free Radical Scavenging Efficacy in Polymer Electrolytes. *ACS Appl. Mater. Interfaces* **2012**, *4* (10), 5098−5102.
(39) Chen, S. Y.; Tsai, C. H.; Huang, M. Z.; Yan, D. C.; Huang, T. W.; Gloter, A.; Chen, C. L.; Lin, H. J.; Chen, C. T.; Dong, C. L. Concentration Dependence of Oxygen Vacancy on the Magnetism of CeO_2 Nanoparticles. *J. Phys. Chem. C* **2012**, *116* (15), 8707−8713.
(40) Della Mea, G. B.; Matte, L. P.; Thill, A. S.; Lobato, F. O.; Benvenutti, E. V.; Arenas, L. T.; Jürgensen, A.; Hergenröder, R.; Poletto, F.; Bernardi, F. Tuning the Oxygen Vacancy Population of Cerium Oxide (CeO_{2-X}, $0 < X < 0.5$) Nanoparticles. *Appl. Surf. Sci.* **2017**, *422*, 1102−1112.
(41) Yuan, F. L.; Zhang, Y. W.; Weber, W. J. Vacancy-Vacancy Interaction Induced Oxygen Diffusivity Enhancement in Undoped Nonstoichiometric Ceria. *J. Phys. Chem. C* **2015**, *119* (23), 13153−13159.
(42) Xiao, Z. R.; Zhang, X. W.; Hou, F.; Wu, C.; Wang, L.; Li, G. Z. Tuning Metal-Support Interaction and Oxygen Vacancies of Ceria Supported Nickel Catalysts by Tb Doping for N-Dodecane Steam Reforming. *Appl. Surf. Sci.* **2020**, *503*, No. 144319.
(43) Lohrenscheit, M.; Hess, C. Direct Evidence for the Participation of Oxygen Vacancies in the Oxidation of Carbon Monoxide over Ceria-Supported Gold Catalysts by Using Operando Raman Spectroscopy. *ChemCatChem.* **2016**, *8* (3), 523−526.
(44) Weststrate, C. J.; Westerstrom, R.; Lundgren, E.; Mikkelsen, A.; Andersen, J. N.; Resta, A. Influence of Oxygen Vacancies on the Properties of Ceria-Supported Gold. *J. Phys. Chem. C* **2009**, *113* (2), 724−728.
(45) Yang, S. C.; Pang, S. H.; Sulmonetti, T. P.; Su, W. N.; Lee, J. F.; Hwang, B. J.; Jones, C. W. Synergy between Ceria Oxygen Vacancies and Cu Nanoparticles Facilitates the Catalytic Conversion of CO_2 to CO under Mild Conditions. *ACS Catal.* **2018**, *8* (12), 12056−12066.
(46) Hernández, N. C.; Grau-Crespo, R.; de Leeuw, N. H.; Sanz, J. F. Electronic Charge Transfer between Ceria Surfaces and Gold Adatoms: A GGA Plus U Investigation. *Phys. Chem. Chem. Phys.* **2009**, *11* (26), 5246−5252.
(47) Fabris, S.; Vicario, G.; Balducci, G.; de Gironcoli, S.; Baroni, S. Electronic and Atomistic Structures of Clean and Reduced Ceria Surfaces. *J. Phys. Chem. B* **2005**, *109* (48), 22860−22867.
(48) Bui, H. T.; Weon, S.; Bae, J. W.; Kim, E. J.; Kim, B.; Ahn, Y. Y.; Kim, K.; Lee, H.; Kim, W. Oxygen Vacancy Engineering of Cerium Oxide for the Selective Photocatalytic Oxidation of Aromatic Pollutants. *J. Hazard. Mater.* **2021**, *404*, No. 123976.
(49) Xiao, M. L.; Han, D. W.; Yang, X. Q.; Tchinda, N. T.; Du, L.; Guo, Y. C.; Wei, Y. C.; Yu, X. L.; Ge, M. F. Ni-Doping-Induced Oxygen Vacancy in Pt-CeO_2 Catalyst for Toluene Oxidation: Enhanced Catalytic Activity, Water-Resistance, and SO_2-Tolerance. *Appl. Catal., B* **2023**, *323*, No. 122173.
(50) Yang, C. M.; Lu, Y. X.; Zhang, L.; Kong, Z. J.; Yang, T. Y.; Tao, L.; Zou, Y. Q.; Wang, S. Y. Defect Engineering on CeO_2-Based Catalysts for Heterogeneous Catalytic Applications. *Small Struct.* **2021**, *2* (12), No. 2100058.
(51) Xiao, Z. R.; Li, Y. T.; Hou, F.; Wu, C.; Pan, L.; Zou, J. J.; Wang, L.; Zhang, X. W.; Liu, G. Z.; Li, G. Z. Engineering Oxygen Vacancies and

https://doi.org/10.1021/jacsau.5c00095
JACS Au 2025, 5, 1549−1569

Nickel Dispersion on CeO_2 by Pr Doping for Highly Stable Ethanol Steam Reforming. *Appl. Catal. B: Environ.* **2019**, *258*, No. 117940.
(52) Han, Z. K.; Yang, Y. Z.; Zhu, B. E.; Ganduglia-Pirovano, M. V.; Gao, Y. Unraveling the Oxygen Vacancy Structures at the Reduced CeO_2(111) Surface. *Phys. Rev. Mater.* **2018**, *2* (3), No. 035802.
(53) Kullgren, J. Oxygen Vacancy Chemistry in Ceria. *PhD Thesis*; Uppsala University, 2012.
(54) Nolan, M. Enhanced Oxygen Vacancy Formation in Ceria (111) and (110) Surfaces Doped with Divalent Cations. *J. Mater. Chem.* **2011**, *21* (25), 9160−9168.
(55) Zacherle, T.; Schriever, A.; De Souza, R. A.; Martin, M. Ab Initioanalysis of the Defect Structure of Ceria. *Phys. Rev. B* **2013**, *87* (13), No. 134104.
(56) Esch, F.; Fabris, S.; Zhou, L.; Montini, T.; Africh, C.; Fornasiero, P.; Comelli, G.; Rosei, R. Electron Localization Determines Defect Formation on Ceria Substrates. *Science* **2005**, *309* (5735), 752−755.
(57) Campbell, C. T.; Peden, C. H. F. Chemistry - Oxygen Vacancies and Catalysis on Ceria Surfaces. *Science* **2005**, *309* (5735), 713−714.
(58) Murgida, G. E.; Ferrari, V.; Llois, A. M.; Ganduglia-Pirovano, M. V. Reduced CeO_2(111) Ordered Phases as Bulk Terminations: Introducing the Structure of Ce_3O_5. *Phys. Rev. Mater.* **2018**, *2* (8), No. 083609.
(59) Olbrich, R.; Murgida, G. E.; Ferrari, V.; Barth, C.; Llois, A. M.; Reichling, M.; Ganduglia-Pirovano, M. V. Surface Stabilizes Ceria in Unexpected Stoichiometry. *J. Phys. Chem. C* **2017**, *121* (12), 6844−6851.
(60) Hull, S.; Norberg, S. T.; Ahmed, I.; Eriksson, S. G.; Marrocchelli, D.; Madden, P. A. Oxygen Vacancy Ordering within Anion-Deficient Ceria. *J. Solid State Chem.* **2009**, *182* (10), 2815−2821.
(61) Jiang, Y.; Adams, J. B.; van Schilfgaarde, M. Density-Functional Calculation of CeO_2 surfaces and Prediction of Effects of Oxygen Partial Pressure and Temperature on Stabilities. *J. Chem. Phys.* **2005**, *123* (6), 064701.
(62) Ou, D. R.; Mori, T.; Ye, F.; Zou, J.; Auchterlonie, G.; Drennan, J. Oxygen-Vacancy Ordering in Lanthanide-Doped Ceria: Dopant-Type Dependence and Structure Model. *Phys. Rev. B* **2008**, *77* (2), No. 024108.
(63) Ou, D. R.; Mori, T.; Ye, F.; Kobayashi, T.; Zou, J.; Auchterlonie, G.; Drennan, J. Oxygen Vacancy Ordering in Heavily Rare-Earth-Doped Ceria. *Appl. Phys. Lett.* **2006**, *89* (17), No. 171911.
(64) Hu, Z. P.; Metiu, H. Effect of Dopants on the Energy of Oxygen-Vacancy Formation at the Surface of Ceria: Local or Global? *J. Phys. Chem. C* **2011**, *115* (36), 17898−17909.
(65) Dholabhai, P. P.; Adams, J. B.; Crozier, P.; Sharma, R. Oxygen Vacancy Migration in Ceria and Pr-Doped Ceria: A DFT Plus U Study. *J. Chem. Phys.* **2010**, *132* (9), No. 094104.
(66) Guo, M.; Lu, J. Q.; Wu, Y. N.; Wang, Y. J.; Luo, M. F. Uv and Visible Raman Studies of Oxygen Vacancies in Rare-Earth-Doped Ceria. *Langmuir* **2011**, *27* (7), 3872−3877.
(67) Torbrügge, S.; Reichling, M.; Ishiyama, A.; Morita, S.; Custance, O. Evidence of Subsurface Oxygen Vacancy Ordering on Reduced CeO_2(111). *Phys. Rev. Lett.* **2007**, *99* (5), No. 056101.
(68) Zhang, K.; Li, G. X.; Zou, C.; Chen, S. Y.; Li, S. D.; Han, Z. K.; Jiang, Y.; Yuan, W. T.; Yang, H. S.; Ganduglia-Pirovano, M. V.; Wang, Y. A CeO_2(100) Surface Reconstruction Unveiled by in Situ Stem and Particle Swarm Optimization Techniques. *Sci. Adv.* **2024**, *10* (32), No. eadn7904.
(69) Varenik, M.; Cohen, S.; Wachtel, E.; Frenkel, A. I.; Nino, J. C.; Lubomirsky, I. Oxygen Vacancy Ordering and Viscoelastic Mechanical Properties of Doped Ceria Ceramics. *Scr. Mater.* **2019**, *163*, 19−23.
(70) Burbano, M.; Norberg, S. T.; Hull, S.; Eriksson, S. G.; Marrocchelli, D.; Madden, P. A.; Watson, G. W. Oxygen Vacancy Ordering and the Conductivity Maximum in Y_2O_3-Doped CeO_2. *Chem. Mater.* **2012**, *24* (1), 222−229.
(71) Nolan, M.; Grigoleit, S.; Sayle, D. C.; Parker, S. C.; Watson, G. W. Density Functional Theory Studies of the Structure and Electronic Structure of Pure and Defective Low Index Surfaces of Ceria. *Surf. Sci.* **2005**, *576* (1), 217−229.
(72) Castleton, C. W. M.; Lee, A.; Kullgren, J. Benchmarking Density Functional Theory Functionals for Polarons in Oxides: Properties of CeO_2. *J. Phys. Chem. C* **2019**, *123* (9), 5164−5175.
(73) Da Silva, J. L. F.; Ganduglia-Pirovano, M. V.; Sauer, J.; Bayer, V.; Kresse, G. Hybrid Functionals Applied to Rare-Earth Oxides: The Example of Ceria. *Phys. Rev. B* **2007**, *75* (4), No. 045121.
(74) Du, D.; Wolf, M. J.; Hermansson, K.; Broqvist, P. Screened Hybrid Functionals Applied to Ceria: Effect of Fock Exchange. *Phys. Rev. B* **2018**, *97* (23), No. 235203.
(75) Graciani, J.; Márquez, A. M.; Plata, J. J.; Ortega, Y.; Hernández, N. C.; Meyer, A.; Zicovich-Wilson, C. M.; Sanz, J. F. Comparative Study on the Performance of Hybrid DFT Functionals in Highly Correlated Oxides: The Case of CeO_2 and Ce_2O_3. *J. Chem. Theory Comput.* **2011**, *7* (1), 56−65.
(76) Hay, P. J.; Martin, R. L.; Uddin, J.; Scuseria, G. E. Theoretical Study of CeO_2 and Ce_2O_3 using a Screened Hybrid Density Functional. *J. Chem. Phys.* **2006**, *125* (3), No. 034712.
(77) Han, X. P.; Amrane, N.; Zhang, Z. S.; Benkraouda, M. Oxygen Vacancy Ordering and Electron Localization in CeO_2: Hybrid Functional Study. *J. Phys. Chem. C* **2016**, *120* (25), 13325−13331.
(78) Ganduglia-Pirovano, M. V.; Murgida, G. E.; Ferrari, V.; Llois, A. M. Oxygen Vacancy Ordering and Electron Localization in CeO_2: Hybrid Functional Study. *J. Phys. Chem. C* **2017**, *121* (38), 21080−21083.
(79) Ganduglia-Pirovano, M. V.; Da Silva, J. L. F.; Sauer, J. Density-Functional Calculations of the Structure of near-Surface Oxygen Vacancies and Electron Localization on CeO_2(111). *Phys. Rev. Lett.* **2009**, *102* (2), No. 026101.
(80) Huang, M.; Fabris, S. Co Adsorption and Oxidation on Ceria Surfaces from DFT+U Calculations. *J. Phys. Chem. C* **2008**, *112* (23), 8643−8648.
(81) Capdevila-Cortada, M.; Lodziana, Z.; López, N. Performance of DFT Plus U Approaches in the Study of Catalytic Materials. *ACS Catal.* **2016**, *6* (12), 8370−8379.
(82) Loschen, C.; Carrasco, J.; Neyman, K. M.; Illas, F. First-Principles LDA Plus U and GGA Plus U Study of Cerium Oxides: Dependence on the Effective U Parameter. *Phys. Rev. B* **2007**, *75* (3), No. 035115.
(83) Zhang, Y. J.; Cai, H. B.; Han, Z. K.; Li, H.; Gao, Y. Fluxionality of Electronic Structures of Supported Metal Catalysts Driven by the Fluctuational Electronic Configurations of the Substrate. *J. Phys. Chem. C* **2024**, *128* (49), 20940−20946.
(84) Zhang, Y.; Han, Z.-K.; Zhu, B.; Hu, X.; Troppenz, M.; Rigamonti, S.; Li, H.; Draxl, C.; Ganduglia-Pirovano, M. V.; Gao, Y. Decoupling Many-Body Interactions in the CeO_2(111) Oxygen Vacancy Structure with Statistical Learning and Cluster Expansion. *Nanoscale* **2025**, *17*, 4531.
(85) Li, Z.; Xu, N.; Zhang, Y. J.; Liu, W.; Wang, J. Q.; Ma, M. L.; Fu, X. L.; Hu, X. J.; Xu, W. W.; Han, Z. K. Unveiling the Structure of Oxygen Vacancies in Bulk Ceria and the Physical Mechanisms Behind Their Formation. *J. Phys. Chem. Lett.* **2024**, *15* (22), 5868−5874.
(86) Xu, N.; Xu, L.; Wang, Y.; Liu, W.; Xu, W. W.; Hu, X. J.; Han, Z. K. Unraveling the Formation of Oxygen Vacancies on the Surface of Transition Metal-Doped Ceria Utilizing Artificial Intelligence. *Nanoscale* **2024**, *16* (20), 9853−9860.
(87) Zhou, L.; Fu, X. P.; Wang, R. X.; Wang, C. X.; Luo, F.; Yan, H.; He, Y.; Jia, C. J.; Li, J.; Liu, J. C. Dynamic Phase Transitions Dictate the Size Effect and Activity of Supported Gold Catalysts. *Sci. Adv.* **2024**, *10* (51), DOI: 10.1126/sciadv.adr4145.
(88) Liu, J. C.; Luo, L. L.; Xiao, H.; Zhu, J. F.; He, Y.; Li, J. Metal Affinity of Support Dictates Sintering of Gold Catalysts. *J. Am. Chem. Soc.* **2022**, *144* (45), 20601−20609.
(89) Shi, J.; Ren, Q.; Gao, Y. Accelerating Global Optimization of Cerium Oxide Nanocluster Structures with High-Dimensional Neural Network Potential. *J. Phys. Chem. A* **2025**, *129*, 2190.
(90) Murgida, G. E.; Ganduglia-Pirovano, M. V. Evidence for Subsurface Ordering of Oxygen Vacancies on the Reduced CeO_2(111) Surface Using Density-Functional and Statistical Calculations. *Phys. Rev. Lett.* **2013**, *110* (24), No. 246101.

https://doi.org/10.1021/jacsau.5c00095
JACS Au 2025, 5, 1549−1569

(91) Pérez-Bailac, P.; Lustemberg, P. G.; Ganduglia-Pirovano, M. V. Facet-Dependent Stability of near-Surface Oxygen Vacancies and Excess Charge Localization at CeO_2 Surfaces. *J. Phys.: Condens. Matter* **2021**, *33* (50), No. 504003.
(92) Trovarelli, A.; Llorca, J. Ceria Catalysts at Nanoscale: How Do Crystal Shapes Shape Catalysis? *ACS Catal.* **2017**, *7* (7), 4716−4735.
(93) Yang, Z. X.; Yu, X. H.; Lu, Z. S.; Li, S. F.; Hermansson, K. Oxygen Vacancy Pairs on CeO_2(110): A DFT + U Study. *Phys. Lett. A* **2009**, *373* (31), 2786−2792.
(94) Herschend, B.; Baudin, M.; Hermansson, K. Electronic Structure of the CeO_2(110) Surface Oxygen Vacancy. *Surf. Sci.* **2005**, *599* (1−3), 173−186.
(95) Kumari, N.; Haider, M. A.; Agarwal, M.; Sinha, N.; Basu, S. Role of Reduced CeO_2(110) Surface for CO_2 Reduction to CO and Methanol. *J. Phys. Chem. C* **2016**, *120* (30), 16626−16635.
(96) Qin, Y. Y.; Su, Y. Q. A Dft Study on Heterogeneous Pt/CeO_2(110) Single Atom Catalysts for CO Oxidation. *ChemCatChem.* **2021**, *13* (17), 3857−3863.
(97) Ji, W. H.; Wang, N.; Li, Q.; Zhu, H.; Lin, K.; Deng, J. X.; Chen, J.; Zhang, H. J.; Xing, X. R. Oxygen Vacancy Distributions and Electron Localization in a CeO_2(100) Nanocube. *Inorg. Chem. Front.* **2022**, *9* (2), 275−283.
(98) Zhong, S. H.; Lu, G. Z.; Gong, X. Q. A DFT Plus U Study of the Structures and Reactivities of Polar CeO_2(100) Surfaces. *Chin. J. of Catal.* **2017**, *38* (7), 1138−1147.
(99) Zhou, C. Y.; Wang, D.; Gong, X. Q. A DFT Plus Urevisit of Reconstructed CeO_2(100) Surfaces: Structures, Thermostabilities and Reactivities. *Phys. Chem. Chem. Phys.* **2019**, *21* (36), 19987−19994.
(100) Nowakowski, L.; Zasada, F.; Gryboś, J.; Sojka, Z. Orbital Resolution of the Reconstruction of CeO_2(100) Facet−Hybrid-DFT and COHP Investigations Supported by HR-TEM Imaging. *J. Phys. Chem. C* **2025**, *129*, 2165.
(101) Zhang, W.; Pu, M.; Lei, M. Theoretical Studies on the Stability and Reactivity of the Metal-Doped CeO_2(100) Surface: Toward H_2 Dissociation and Oxygen Vacancy Formation. *Langmuir* **2020**, *36* (21), 5891−5901.
(102) Xu, S. T.; Chen, X. X.; Zhan, S. J.; Tian, S. H.; Xiong, Y. Fe Doped CeO_2 Nanocubes with the Exposure of Active (100) Facets for Photocatalytic Ozonation of 4-Chlorophenol under Solar Irradiation. *J. Chem. Technol. Biotechnol.* **2021**, *96* (6), 1523−1532.
(103) Li, H. Y.; Wang, H. F.; Gong, X. Q.; Guo, Y. L.; Guo, Y.; Lu, G. Z.; Hu, P. Multiple Configurations of the Two Excess 4f Electrons on Defective CeO_2(111): Origin and Implications. *Phys. Rev. B* **2009**, *79* (19), No. 193401.
(104) Jerratsch, J. F.; Shao, X.; Nilius, N.; Freund, H. J.; Popa, C.; Ganduglia-Pirovano, M. V.; Burow, A. M.; Sauer, J. Electron Localization in Defective Ceria Films: A Study with Scanning-Tunneling Microscopy and Density-Functional Theory. *Phys. Rev. Lett.* **2011**, *106* (24), No. 246801.
(105) Kullgren, J.; Wolf, M. J.; Castleton, C. W. M.; Mitev, P.; Briels, W. J.; Hermansson, K. Oxygen Vacancies Versus Fluorine at CeO_2(111): A Case of Mistaken Identity? *Phys. Rev. Lett.* **2014**, *112* (15), No. 156102.
(106) Wu, X. P.; Gong, X. Q. Clustering of Oxygen Vacancies at CeO_2(111): Critical Role of Hydroxyls. *Phys. Rev. Lett.* **2016**, *116* (8), No. 086102.
(107) Wu, X. P.; Gong, X. Q.; Lu, G. Z. Role of Oxygen Vacancies in the Surface Evolution of H at CeO_2(111): A Charge Modification Effect. *Phys. Chem. Chem. Phys.* **2015**, *17* (5), 3544−3549.
(108) Kullgren, J.; Wolf, M. J.; Mitev, P. D.; Hermansson, K.; Briels, W. J. DFT-Based Monte Carlo Simulations of Impurity Clustering at CeO_2(111). *J. Phys. Chem. C* **2017**, *121* (28), 15127−15134.
(109) Han, Z. K.; Duan, X. Y.; Li, X. Y.; Zhang, D. W.; Gao, Y. The Dynamic Interplay between Water and Oxygen Vacancy at the near-Surface of Ceria. *J. Phys.: Condens. Matter* **2021**, *33* (42), No. 424001.
(110) Zhu, L.; Jin, X.; Zhang, Y. Y.; Du, S. X.; Liu, L.; Rajh, T.; Xu, Z.; Wang, W. L.; Bai, X. D.; Wen, J. G.; Wang, L. F. Visualizing Anisotropic Oxygen Diffusion in Ceria under Activated Conditions. *Phys. Rev. Lett.* **2020**, *124* (5), No. 056002.
(111) Pang, D. W.; Li, W.; Zhang, N. Q.; He, H.; Mao, S. C.; Chen, Y. H.; Cao, L. W.; Li, C.; Li, A.; Han, X. D. Direct Observation of Oxygen Vacancy Formation and Migration over Ceria Surface by in Situenvironmental Transmission Electron Microscopy. *J. Rare Earths* **2024**, *42* (4), 676−682.
(112) Waldow, S. P.; De Souza, R. A. Is Excess Faster Than Deficient? A Molecular-Dynamics Study of Oxygen-Interstitial and Oxygen-Vacancy Diffusion in CeO_2. *J. Phys. Energy* **2020**, *2* (2), No. 024001.
(113) Li, H. Y.; Wang, H. F.; Guo, Y. L.; Lu, G. Z.; Hu, P. Exchange between Sub-Surface and Surface Oxygen Vacancies on CeO_2 (111): A New Surface Diffusion Mechanism. *Chem. Commun.* **2011**, *47* (21), 6105−6107.
(114) Ahn, K.; Chung, Y. C.; Yoon, K. J.; Son, J. W.; Kim, B. K.; Lee, H. W.; Lee, J. H. Lattice-Strain Effect on Oxygen Vacancy Formation in Gadolinium-Doped Ceria. *J. Electroceramics* **2014**, *32* (1), 72−77.
(115) Liu, X. J.; Wei, S. C.; Cao, S. Y.; Zhang, Y. G.; Xue, W.; Wang, Y. J.; Liu, G. H.; Li, J. D. Lattice Strain with Stabilized Oxygen Vacancies Boosts Ceria for Robust Alkaline Hydrogen Evolution Outperforming Benchmark Pt. *Adv. Mater.* **2024**, *36* (33), No. 2405970.
(116) Ma, D. W.; Lu, Z. S.; Tang, Y. N.; Li, T. X.; Tang, Z. J.; Yang, Z. X. Effect of Lattice Strain on the Oxygen Vacancy Formation and Hydrogen Adsorption at CeO_2(111) Surface. *Phys. Lett. A* **2014**, *378* (34), 2570−2575.
(117) Han, Z. K.; Zhang, L.; Liu, M. L.; Ganduglia-Pirovano, M. V.; Gao, Y. The Structure of Oxygen Vacancies in the near-Surface of Reduced CeO_2(111) under Strain. *Front. Chem.* **2019**, *7*, 436.
(118) Rushton, M. J. D.; Chroneos, A. Impact of Uniaxial Strain and Doping on Oxygen Diffusion in CeO_2. *Sci. Rep.* **2014**, *4*, 6068.
(119) Balaji Gopal, C.; Garcia-Melchor, M.; Lee, S. C.; Shi, Y.; Shavorskiy, A.; Monti, M.; Guan, Z.; Sinclair, R.; Bluhm, H.; Vojvodic, A.; Chueh, W. C. Equilibrium Oxygen Storage Capacity of Ultrathin $CeO_{2-\Delta}$ Depends Non-Monotonically on Large Biaxial Strain. *Nat. Commun.* **2017**, *8*, No. 15360.
(120) Babu, S.; Thanneeru, R.; Inerbaev, T.; Day, R.; Masunov, A. E.; Schulte, A.; Seal, S. Dopant-Mediated Oxygen Vacancy Tuning in Ceria Nanoparticles. *Nanotechnology* **2009**, *20* (8), No. 085713.
(121) Shehata, N.; Meehan, K.; Hudait, M.; Jain, N. Control of Oxygen Vacancies and Ce+3 Concentrations in Doped Ceria Nanoparticles Via the Selection of Lanthanide Element. *J. Nanopart. Res.* **2012**, *14* (10), 1173.
(122) Vinodkumar, T.; Rao, B. G.; Reddy, B. M. Influence of Isovalent and Aliovalent Dopants on the Reactivity of Cerium Oxide for Catalytic Applications. *Catal. Today* **2015**, *253*, 57−64.
(123) Yang, C. W.; Yu, X. J.; Heissler, S.; Nefedov, A.; Colussi, S.; Llorca, J.; Trovarelli, A.; Wang, Y. M.; Wöll, C. Surface Faceting and Reconstruction of Ceria Nanoparticles. *Angew. Chem., Int. Ed.* **2017**, *56* (1), 375−379.
(124) Bhatta, U. M.; Ross, I. M.; Sayle, T. X. T.; Sayle, D. C.; Parker, S. C.; Reid, D.; Seal, S.; Kumar, A.; Möbus, G. Cationic Surface Reconstructions on Cerium Oxide Nanocrystals: An Aberration-Corrected HRTEM Study. *ACS Nano* **2012**, *6* (1), 421−430.
(125) Yang, C. W.; Capdevila-Cortada, M.; Dong, C. Y.; Zhou, Y.; Wang, J. J.; Yu, X. J.; Nefedov, A.; Heissler, S.; López, N.; Shen, W. J.; Wöll, C.; Wang, Y. M. Surface Refaceting Mechanism on Cubic Ceria. *J. Phys. Chem. Lett.* **2020**, *11* (18), 7925−7931.
(126) Duchon, T.; Dvorák, F.; Aulická, M.; Stetsovych, V.; Vorokhta, M.; Mazur, D.; Veltruská, K.; Skála, T.; Myslivecek, J.; Matolínová, I.; Matolín, V. Ordered Phases of Reduced Ceria as Epitaxial Films on Cu(111). *J. Phys. Chem. C* **2014**, *118* (1), 357−365.
(127) Pan, Y.; Nilius, N.; Stiehler, C.; Freund, H. J.; Goniakowski, J.; Noguera, C. Ceria Nanocrystals Exposing Wide (100) Facets: Structure and Polarity Compensation. *Adv. Mater. Inter.* **2014**, *1* (9), No. 1400404.
(128) Capdevila-Cortada, M.; López, N. Entropic Contributions Enhance Polarity Compensation for CeO_2(100) Surfaces. *Nat. Mater.* **2017**, *16* (3), 328.
(129) Gonzalez-DelaCruz, V. M.; Holgado, J. P.; Pereníguez, R.; Caballero, A. Morphology Changes Induced by Strong Metal-Support

https://doi.org/10.1021/jacsau.5c00095
JACS Au 2025, 5, 1549−1569

Interaction on a Ni-Ceria Catalytic System. *J. Catal.* **2008**, *257* (2), 307−314.
(130) Parastaev, A.; Muravev, V.; Huertas Osta, E.; van Hoof, A. J. F.; Kimpel, T. F.; Kosinov, N.; Hensen, E. J. M. Boosting CO_2 Hydrogenation Via Size-Dependent Metal-Support Interactions in Cobalt/Ceria-Based Catalysts. *Nat. Catal.* **2020**, *3* (6), 526−533.
(131) Farmer, J. A.; Campbell, C. T. Ceria Maintains Smaller Metal Catalyst Particles by Strong Metal-Support Bonding. *Science* **2010**, *329* (5994), 933−936.
(132) Cargnello, M.; Doan-Nguyen, V. V. T.; Gordon, T. R.; Diaz, R. E.; Stach, E. A.; Gorte, R. J.; Fornasiero, P.; Murray, C. B. Control of Metal Nanocrystal Size Reveals Metal-Support Interface Role for Ceria Catalysts. *Science* **2013**, *341* (6147), 771−773.
(133) Han, Z. K.; Wang, Y. G.; Gao, Y. Catalytic Role of Vacancy Diffusion in Ceria Supported Atomic Gold Catalyst. *Chem. Commun.* **2017**, *53* (65), 9125−9128.
(134) Cai, H.; Zhang, Y.; Tang, Q.; Han, Z.-K.; Gao, Y. Exploring Structures of Pd Clusters on Hydrogenated Ceria Surface Using High-Dimensional Neural Network Potential. *Appl. Surf. Sci.* **2025**, *692*, No. 162780.
(135) Han, Z. K.; Gao, Y. A 2d-3d Structure Transition of Gold Clusters on CeO_{2-X}(111) Surfaces and Its Influence on CO and O_2 Adsorption: A Comprehensive DFT Plus U Investigation. *Nanoscale* **2015**, *7* (1), 308−316.

https://doi.org/10.1021/jacsau.5c00095
JACS Au 2025, 5, 1549−1569